Theory and Applications of Goos-Hänchen Shift

Based On Guided Mode Resonance

BY

RUI YANG
M.S. in Physics, University of Illinois at Chicago, USA, 2012
B.S. in Physics, Shandong University, China, 2011

THESIS

Submitted as partial fulfillment of the requirements
for the degree of Doctor of Philosophy in Electrical and Computer Engineering
in the Graduate College of the
University of Illinois at Chicago, 2016

Chicago, Illinois

Defense Committee:

Danilo Erricolo, Chair and Advisor
Jingjing Li, Advisor
Wolfgang-Martin Boerner
Wei Wu, University of Southern California
Jingyi Wang, Avago Technologies

To

my parents,

Yang Guangtian & Shi Changgui

ACKNOWLEDGMENTS

This work could have not be accomplished without the support of many people. First and foremost, I would like to express my sincere gratitude to my advisor Dr. Jingjing Li, who dedicated and patiently taught and shared not only knowledge of science, but also experience in life. I must thank my co-advisor Prof. Danilo Erricolo, who has always been supportive and helped me out of tremendous difficulty. I cannot image how much more problems I would have faced without his support. I have to thank Prof. Wolfgang-Martin Boerner for his dedication in proof reading my thesis and education in thinking which will benefit me for my entire life. Dr. Jingyi Wang deserves my great appreciation for the invaluable discussion and seeking me great opportunities. I would also like to thank my committee member, Prof. Wei Wu for his guidance of this thesis.

I could have not made it today without my parents' decades of sacrifices and support. My father, Yang Guangtian and my mother, Shi Changgui deserve my deepest appreciation for raising and educating me. After five years apart, their hair had turned gray. I have to thank my uncle, Wancheng Mao and aunt, Dewan Duan, who took care of me like parents and gave me another home in the United States. Last but not the least, I need to thank my colleagues and friends at UIC, Farhad Farzami, Shanshan Zhao, Tadahiro Neghish, Yangqing Liu, Omid Manoochehri, Yi Lan, Bin Shi, Yang Hao, Boyan Huang, Ting Yuan and Bo Ling for their priceless friendship and supports.

RY

TABLE OF CONTENTS

TABLE OF CONTENTS (Continued)

CHAPTER **PAGE**

LIST OF FIGURES

LIST OF FIGURES (Continued)

LIST OF FIGURES (Continued)

FIGURE **PAGE**

LIST OF FIGURES (Continued)

LIST OF ABBREVIATIONS

EM	Electromagnetic
PEC	Perfect Electrical Conductor
EIT	Electromagnetically Induced Transparency
GH Shift	Goos-Hänchen Shift
TIR	Total Internal Reflection
FTIR	Frustrated Total Internal Reflection
GMR	Guided Mode Resonance
MEEP	MIT Electromagnetic Equation Propagation
RCWA	Rigorous Coupled Wave Analysis
FDTD	Finite Difference Time Domain analysis

SUMMARY

Integrated optics has been seen as the next generation of network and processor technology. It provides advantages such as higher performance, increased bandwidth and speed, more compact size, lower coupling losses, lower package cost and lower power consumption. However, the research slowly paves its way with limited progress. The difficulty are such but no limited to the complexity of material system for photonics, the fabrication precision limits, the quantum mechanical limits, etc.. Enormous efforts and approaches have been contributed to the building blocks of integrated optics. This dissertation contributes to developing one building block of integrated optics through a new interpretation of the Goos-Hänchen shift that resulted in the first grating structures that potentially display a high signal to noise ratio to enable many applications.

In this dissertation, an innovative approach to describe and implement the Goos-Hänchen Shift theory and application in the nano photonics area is presented. The Goos-Hänchen shift is an optical phenomenon in which linearly polarized light experiences certain lateral shift under total internal reflection (TIR). The theory to explain Goos-Hänchen (GH) shift has undergone a long time to mature and is still ongoing. The discussion resulted in mathematical and physical aspects which are the stationary phase and evanescent wave penetration approach, respectively. However, problems showed up for the validity to extend the understanding of negative GH shift, which is theoretically predicted and was experimentally observed in recent years. Hence, it brought renewed interests in realization and theoretical understanding of the

negative shift property, particularly with the study of resonance features such as surface plasmonic resonance and metamaterial (a negative permittivity or permeability material realized by the electromagnetic resonance concept). Besides these two approaches, this thesis discusses another approach using dielectric gratings to realize giant negative or positive GH shift taking advantage of the guided mode resonance (GMR). Theoretical analysis of the physical property of GH shift will be presented to understand the giant and negative anomaly from a energy flow point of view. Further, implementation of GH shift to the nonlinear optical phenomenon stability is discussed for optical switch applications. The application of the guided mode resonance includes controlling the dispersion of a waveguide in order to stop optical signal flow, which will be presented in this dissertation.

The thesis is organized in the following: Chapter 1 provides an introduction of the GH shift and current trends in research; Chapter 2 describes the details of guided mode resonance; in Chapter 3, negative or positive and giant GH shift realization based on the guided mode resonance is presented; followed by Chapter 4 exhibits application to the optical bistability phenomenon; Chapter 5 demonstrates another application of the giant negative GH shift to achieve broad spectrum light signal trapping, the "*trapped rainbow*" and Chapter 6 concludes this thesis and discusses the future of further study.

CHAPTER 1

INTRODUCTION

When a light beam experiences total internal reflection (TIR), instead of being immediately reflected back, it shifts along the interface at a certain distance. The displacement between the incidence and reflection point is a striking discrepancy with the prediction of geometric optics that light beams are supposed to bounce back directly. Such a lateral displacement between the centers of the incident and reflected beams is called Goos-Hänchen shift, named after its discoverers Hermann Fritz Gustav Goos and Hilda Hänchen in 1947 (1).

One year after the discovery of the Goos-Hänchen shift, Artmman proposed an explanation of such a phenomenon based on an argument of stationary phase (2). He explained that the displacement was due to angular components of the beam experiencing different phase loss at the reflection and he formulated a mathematical expression according to the phase loss. This theoretical work also predicted the different responses for parallel and perpendicular polarizations. Goos and Hänchen then conducted another measurement and verified the polarization dependence in 1949 (3). Artmman's theory was further proven by Wolter in 1950 in good agreement with measurement (4). In addition to the mathematical interpretation, Burke has provided a straight forward model introducing the concept of penetration depth (5). It explains the phenomenon as the beam could penetrate into the lower refractive index media for a certain depth and then be reflected back. Such penetration increases the optical path in the low refractive index media while appearing on the interface as the Goos-Hänchen shift.

The Goos-Hänchen shift has since attracted interests for several decades with considerable amount of efforts focused toward a better understanding of the underlying physical principle, and gained renewed attention in recent years when plasmonic materials and metamaterials were analyzed for implementations in the next generation of nano-processor technology. Goos-Hänchen shift is generally considered as a small position leap forwards due to the delay of the center of a Gaussian beam. However, a negative Goos-Hänchen shift was discovered specifically in the studies of plasmonic and metamaterial surfaces (6; 7; 8). Up to now, the concept has been extended from a small positive shift to giant negative and positive shifts. The condition also has been relaxed from total internal reflection to partial reflection. Sensor schemes based on the Goos-Hänchen shift have been proposed and led to applications in thermal, biomechanical sensoring and wavelength monitoring, etc. The sensitivity of these sensors has a direct relation to the strength of the Goos-Hänchen shift. Hence, for achieving a large Goos-Hänchen shift results in a realistic verification. However, plasmonic or metamaterial have a considerable ohmic loss at the optical frequency which results in a trade-off between the amount of Goos-Hänchen shift and reflectivity. Larger Goos-Hänchen shift values always lead to smaller reflectivity and thus a greater loss of signal to noise ratio. On the other hand, a limited extent of lateral displacement would cost more sensitivity of the optical position sensor. This thesis provides a solution to this still unresolved issue by replacing the metalic material with dielectrics. In the thesis, a one dimensional periodic dielectric grating was designed as a "metasurface" being a function of metamaterials, of which the grating provides the abnormal reflection phase loss that only metamaterial does. It can achieve positive and negative Goos-Hänchen shift while

maintaining the reflectance as 100% based on the Guided Mode Resonance (GMR) inside the grating and prism couplers. GMR is a typical resonance inside subwavelength grating structure. It has been used in broadband reflectors, sensors, cavities, couplers and filters. This study explores the possibility to use GMR for achieving giant Goos-Hänchen shifts. Besides that, more potential use of this grating and the GMR effect were discovered and implemented to certain other applications (9; 10; 11).

1.1 Review of Goos-Hänchen Shift Theory

This section reviews the fundamental conditions for the Goos-Hänchen shift which is the total internal reflection of a light beam. From the Fresnel's law we can state that the complex reflection coefficient for incident angle must be larger than the critical angle. Then, we use Arthmann's equation to derive the general Goos-Hänchen shift for dielectrics. More advanced Goos-Hänchen shift phenomena are discussed leading to current studies.

1.1.1 Reflection Phase Loss of Total Internal Reflection (TIR)

Goos-Hänchen shift, in general, refers to the lateral shift along the interface when a light beam experiences total internal reflection. Total internal reflection is a well-known concept and a light beam will experience and total reflection as long as the incident angle exceeds the critical angle when it travels from a high refractive index media to a lower one. However, while discussing the problem of total internal reflection, most of the interest is typically focused on the magnitude of the reflectivity while little attention is paid to the phase property of the reflection. To give a brief introduction of the TIR, we begin from the Fresnel reflection and transmission formulas of two homogeneous media (12). Equation 1.1 shows both the reflection

coefficients of the perpendicular, 's' and parallel, 'p' polarization for an incident plane wave travelling from medium 1 to medium 2

$$\Gamma_s = \frac{\eta_2 \cos\theta_i - \eta_1 \cos\theta_t}{\eta_2 \cos\theta_i + \eta_1 \cos\theta_t} \tag{1.1a}$$

$$\Gamma_p = \frac{-\eta_1 \cos\theta_i + \eta_2 \cos\theta_t}{\eta_1 \cos\theta_i + \eta_2 \cos\theta_t} \tag{1.1b}$$

Here, η is the lossless wave impedance of each medium, which can be also written as $\eta = \sqrt{\mu/\epsilon}$, where μ is the permeability while ϵ is the permittivity. θ_i and θ_t are incident and transmitted angle respectively. Since for most dielectric media, except for ferromagnetic materials, the permeability $\mu_1 \approx \mu_2 \approx \mu_0$, we may rewrite Snell's law of refraction as:

$$n_1 \sin\theta_i = n_2 \sin\theta_t \tag{1.2}$$

Here n is the refractive index which is $n = \sqrt{\epsilon_r}$. Also, we define $n_r = n_2/n_1$ as the relative refractive index. We can then reduce Equation 1.1 by applying Equation 1.2 to

$$\Gamma_s = \frac{\cos\theta_i - n_r\sqrt{1 - \frac{\sin^2\theta_i}{n_r^2}}}{\cos\theta_i + n_r\sqrt{1 - \frac{\sin^2\theta_i}{n_r^2}}} \tag{1.3a}$$

$$\Gamma_p = \frac{-\cos\theta_i + \frac{1}{n_r}\sqrt{1 - \frac{\sin^2\theta_i}{n_r^2}}}{\cos\theta_i + \frac{1}{n_r}\sqrt{1 - \frac{\sin^2\theta_i}{n_r^2}}} \tag{1.3b}$$

When the incidence angle θ_i exceeds the critical angle, the reflection coefficients for both polarizations become a complex number with a magnitude of 1. The expression can be written as:

$$\Gamma_s = \frac{\cos\theta_i - jn_r\sqrt{\frac{\sin^2\theta_i}{n_r^2} - 1}}{\cos\theta_i + jn_r\sqrt{\frac{\sin^2\theta_i}{n_r^2} - 1}} \tag{1.4a}$$

$$\Gamma_p = \frac{-\cos\theta_i + j\frac{1}{n_r}\sqrt{\frac{\sin^2\theta_i}{n_r^2} - 1}}{\cos\theta_i + j\frac{1}{n_r}\sqrt{\frac{\sin^2\theta_i}{n_r^2} - 1}} \tag{1.4b}$$

Then the reflection coefficient can be expressed as $\Gamma = e^{-j\phi_r}$. Notice here $e^{-j\omega t}$ time harmonic is used through out the dissertation. Using Euler's equation $e^{-j\phi} = \cos\phi - j\sin\phi$, it is easy to derive from Equation 1.4 the reflection phase loss ϕ_r of both polarizations.

$$\phi_r^s = -2\tan^{-1}\left(\frac{\sqrt{\sin^2\theta_i - n_r^2}}{\cos\theta_i}\right) \tag{1.5a}$$

$$\phi_r^p = -2\tan^{-1}\left(\frac{\sqrt{\sin^2\theta_i - n_r^2}}{n_r^2\cos\theta_i}\right) \tag{1.5b}$$

Notice here that Equation 1.5 is only valid for TIR because when the incident angle is below the critical angle, i.e. $\sin\theta_i < n_r$, the reflection coefficient is always a real value, which is apparent from Equation 1.3.

1.1.2 Artmman's Theory of Goos-Hänchen Shift and Its Development

Artmman's theory (2), based on the stationary phase argument, says that the the displacement was due to different reflective phase losses of angular components of the beam. Hence, the

Goos-Hänchen shift can be expressed as the derivative of the reflection phase loss with respect to the beam's lateral wavenumber according to (2) as

$$S = -\frac{d\phi_r}{d\beta} = -\frac{1}{k_1 \cos\theta_i}\frac{d\phi_r}{d\theta_i} \tag{1.6}$$

Here, S is the Goos-Hänchen shift, ϕ_r is the reflection phase loss while β is the lateral wavenumber of the beam. It can be also written in a second form where $k_1 = 2\pi/\lambda_1 = \beta/\cos\theta_i$ is the wavenumber of the media 1 while λ_1 is the wavelength of the beam inside media 1. Based on Artmman's formula (2), the corresponding Goos-Hänchen shift for both perpendicular and parallel polarization can be derived by substituting Equation 1.5 into Equation 1.6:

$$S_s = \frac{\lambda_1}{\pi}\frac{\sin\theta_i}{\sqrt{\sin^2\theta_i - n_r^2}} \tag{1.7a}$$

$$S_p = \frac{n_r^2}{\sin^2\theta_i(1+n_r^2) - n_r^2}S_s \tag{1.7b}$$

In Figure 1, it is clear to see that the expression for the Goos-Hänchen shift diverges near the critical angle. Artmman and Wolter did the early generalization to the near critical angle and more recently Horowitz and Tamir (13) and Lai et al. (14) developed theories involving uniform approximations near the critical angle. These theories further pointed out that there are nonvanishing Goos-Hänchen shifts even for an incident angle below the critical angle, although in the plane wave approximation, discussed above, there is no reflection phase loss for such incidence. The theoretical result reveals also the fact that a light beam having finite width

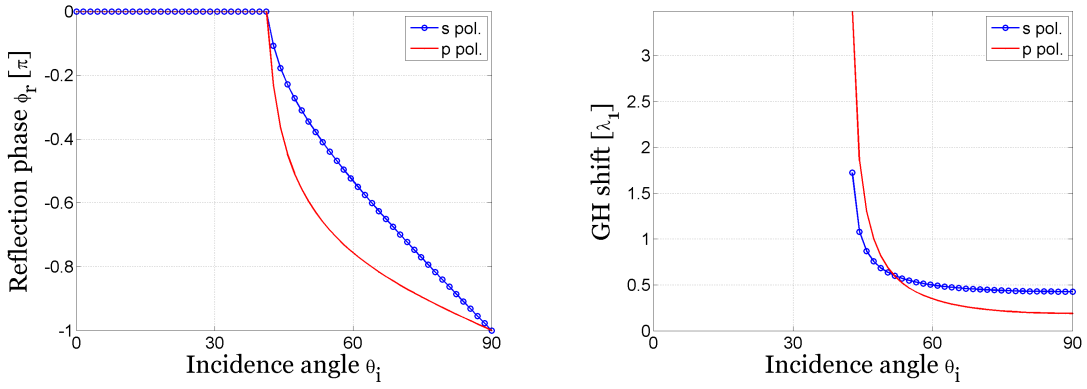

(a) (b)

Figure 1: An example of the reflection phase loss and the Goos-Hänchen shift of a beam with the two media's relative refractive index $n_r = 1.5$. (a) The reflection phase loss response to the incidence angle. (b): The Goos-Hänchen shift response to the incidence angle.

consists of a range of angles of incidence. The angle used in the mathematical expression is regarded as the average or center incidence. At the near critical angle, the incidence beam contains angles experiencing both TIR and normal reflection simultaneously, which refers to a greater Goos-Hänchen shift. The maximum value of the Goos-Hänchen shift is typically of few wavelengths for a beamwidth of hundreds of wavelengths.

Another interesting phenomenon in Figure 1 is the non-vanishing Goos-Hänchen shift at the grazing angle, $\theta_i = 90°$. According to Artmman's theory, the Goos-Hänchen shift does not vanish at the grazing angle which is counter-intuitive. This problem was questioned by Renard in 1964 (15). He then proposed that the Goos-Hänchen shift is related to the lateral energy flow carried by the evanescent wave beyond the interface of the TIR. Finally, Renard achieved

a modified expression for which the Goos-Hänchen shift vanishes at the grazing angle. Later Lotsch also obtained an expression vanishing at the grazing incidence (16), however, the result was questioned and corrected by Carnaglia (17). Carnaglia's suggestion to correct Lotsch's result, in turn, supported Artmman's result that the Goos-Hänchen shift at grazing incidence indeed exists. Lai then supported the result by arguing that Artmman's result is valid between an incidence angle of $\theta_c + \varepsilon$ and $\pi/2 - \varepsilon$, where θ_c is the critical angle and ε is typically on the order of a hundredth of a radian.

A comprehensive model was first introduced by Burke (5). As described in Figure 2, the light ray penetrates the interface to the lower refractive index medium for a certain depth and then is reflected back. As a consequence of the penetration, the light travels an additional distance while on the interface appears as a lateral shift.

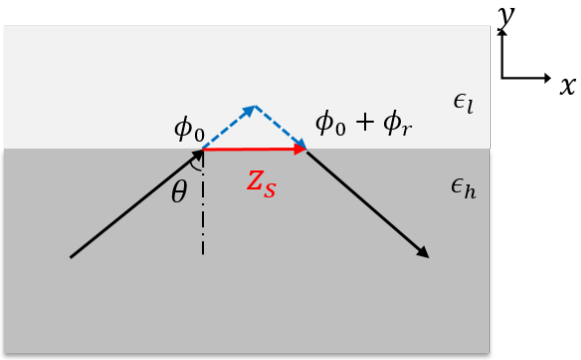

Figure 2: The schematics of a beam penetrating the interface of total internal reflection for a certain depth then being reflected back. The lateral projection of the penetration, z_s, indicates the Goos-Hänchen shift along propagation direction $\hat{x}$.

1.1.3 Review of Negative Goos-Hänchen Shift

The study of the negative Goos-Hänchen shift in TIR was started as early as 1971 (6), which was the first claim that a leaky wave structure can lead to a negative shift. At that time, the amount of negative shift was small and had always been less than a wavelength. A theoretic analysis of reflection at a subwavelength metallic grating further claimed the existence of negative Goos-Hänchen shift (18) later in 1978. Four years later, a striking theoretical result based on Artmman's theory found by Wild and Giles (19), suggested a 2.8 wavelength long negative Goos-Hänchen shift on a germanium/air interface with complex index of refraction. Yet, the authors were not able to provide an explanation to such a phenomenon. Even the detectability of the result was doubted in the same paper for the conducted realistic experiment since the reflectance of the beam is relatively small. Larger negative Goos-Hänchen shift to tens of times the wavelength was achieved theoretically by Lai and Chan (20) on reflection from weakly absorbing media near the Brewster dip. They claimed that for a parallel polarized incident beam across the Brewster angle, the reflection coefficient would have a phase shift of π, which resulted in a large negative Goos-Hänchen shift according to Artmman's theory. The result had an impressive amount of Goos-Hänchen shift of 42.4 wavelength, however, reduces the reflectance to less than 0.01%.

The negative Goos-Hänchen shift gained renewed attention when plasmonic material, photonic crystal and metamaterial were implemented. Berman derived a negative Goos-Hänchen shift in a negative refractive media (left-handed material) for both perpendicular and parallel polarization, while before that it was only achieved with parallel polarization (21). However,

the hypothesis of perfect lensing by a slab of left-handed material described in the paper has not been proven yet. The author left an open question in the end to the possibility of observing a reversed Goos-Hänchen shift. Since that, considerable theoretical analyses of negative Goos-Hänchen shift were carried out as to achieve larger displacements and reflectance (7; 22; 23; 24; 25). In the mean time, the negative Goos-Hänchen shift of the parallel polarized incident beam at a metallic surface had been experimentally observed by Merano et al. (26).

The Goos-Hänchen shift had been generally understood as to account for the penetration of the evanescent field to the other side of the interface (27). This interpretation faces difficulty in explaining the negative Goos-Hänchen shift. Renard explained that the Goos-Hänchen shift is related to the lateral energy flow carried by the evanescent wave beyond the interface of total reflection (15). Whether the Goos-Hänchen shift is positive or negative depends on the direction of the energy flow: When it is in the same direction of the projection of beam propagation direction to the interface, the shift is positive; when the energy flow is the opposite, negative Goos-Hänchen shift happens. This explanation gives an intuitive understanding to the phenomenon, and can perfectly explain the negative Goos-Hänchen shift on plasmonic and metamaterial interfaces.

In addition, a series of theoretical works by Tamir (6; 28) on the relationship between the Goos-Hänchen shift and the leaky mode of multi-layer and periodic structures have been studied. Experimental works demonstrating his theory were carried out much more recently, but mostly on acoustic waves (29; 30; 31).

1.2 Overview

In this thesis, we will introduce a new method based dielectric grating approach that applies to the guided mode resonance for generating large positive and negative Goos-Hänchen shifts. A figure of merit for guided mode resonance would be a high quality factor. We will show that low threshold power bistability can be achieved via the grating-substrate structure. Nonlinear material was then implemented to the device to achieve optical bistablity, an important technique to apply to optical switches and memories. We also will demonstrate the potential of the gratings to control the dispersion of the waveguide via surface dispersion engineering. Exciting phenomena include slow light and trapping broadband light signal spectrum across the visible light range.

CHAPTER 2

REVIEW OF GUIDED MODE RESONANCE

2.1 Introduction

When bringing a diffraction grating and an optical waveguide into proximity, guided modes can be excited to and simultaneously extracted from the waveguide by the diffraction grating. This occurs when the angle of the diffracted mode is matched with that of the guided mode. Such a phenomenon is called guided mode resonance (GMR). In recent years, high contrast gratings have been introduced to functioning as both grating and waveguide, which is called grating waveguide structure. This structure can excite a high quality factor GMR and provide pronounced features. It has advantages such as frequency selectivity, high reflectivity and compact size. One of the features is broadband ultra-high reflectivity ($> 98.5\%$) or transmission (9; 10). It was implemented to vertical-cavity-surface-emitting lasers (VCSELs) instead of the several times bulkier Distributed Bragg Reflector(DBR) (32). Another important application is broadband filters (33; 11). The advantage not only includes high reflection/transmission, but also design feasibility. The quality factor of GMR, which determines the reflectivity, can be determined by the parameters of the high contrast grating. For example, the filling factor of the material and the contrast of the refractive index of the material and the gap, etc.. Also, the size of the grating, especially the period and thickness, is essential for the resonant frequency. GMR can provide different reflection phases by changing the grating size. More interestingly,

it can provide a curved wave front by engineering the phase response. This leads to a planar, single-layer grating lens that can focus light (34). There are many more applications of GMR in sensing technologies and other fields. In this chapter, we will demonstrate the fundamental physics of GMR as the prerequisite knowledge of this thesis. Note that, the detailed field expression derivation are represented in Appendix A.

2.2 Guided Mode Resonance

Guided mode resonance is also named as leak wave resonance or waveguide-mode resonance, which is a phenomenon wherein the guided mode a of waveguide can be excited while simultaneously coupled out using phase-matching elements, such as a diffraction grating. The guided mode resonance is also named as "*leaky mode resonance*", which means the guided wave keeps radiating to the ambient media as the wave propagates. This section introduces the fundamental phenomenon of the guided mode resonance which the diffracted mode of the grating matches with the waveguide mode.

2.2.1 Review of Diffraction Gratings and Slab Waveguide

A classic grating is a one-dimensional periodic structure that consists of equally spaced grooves. According to the Huygens-Fresnel principle, each one of the grooves will act as second light source when a light beam is incident onto the grating surface. Hence diffraction occurs. The function of a classic diffracted grating is to interact with a wave such that it generates a series of additional waves, traveling in different directions which are dependent upon the wavelength and the grating parameters (35).

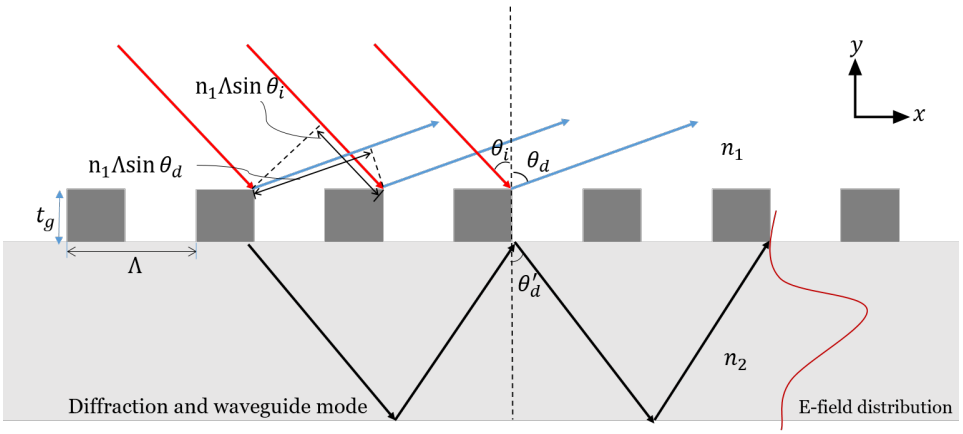

Figure 3: Basic geometry of grating waveguide structure and relevant interference waves. The red line represents the incidence while blue and black lines represent the diffracted waves.

In the original experiment of a normal incident plane wave diffracted by a slit aperture, two second sources, the edges of the slit, scattering light towards a point constructively with each other will be considered in phase. Constructive interference obeys the relation: $d = \lambda / \sin\theta$, where d is the width of the slit, λ is the wavelength, while θ is the transmission angle. This concept can be extended to multi-slit structures, the grating with arbitrary incident angle. Consider a plane wave striking on the grating surface with an incident angle θ_i with respect to the grating grooves, the diffracted angle can be arbitrarily distributed which can be represented by θ_d, shown in Figure 3. Note that the angles of the diffracted waves can be reflection (θ_d) or transmission (θ'_d), respectively. Taking the diffraction reflected back to media 1 as an example, the optical path difference between two adjacent grooves will then be $(n_1 \Lambda \sin\theta_i - n_1 \Lambda \sin\theta_d)$, where Λ is the period of the grating. In order to build up constructive interference between the two adjacent diffracted waves, the optical path difference must be equal to an integer multiple of

the incident light wavelength, or $n_1\Lambda\sin\theta_i - n_1\Lambda\sin\theta_d = m\lambda \quad m = 0, \pm1, \pm2, ...$ The diffracted waves satisfying the relations will be enhanced while those with other angles will experience destructive interference so that the light waves are eventually canceled by each other. The enhanced diffracted waves at specific angles are then called the diffraction modes. Therefore, it is easy to derive the diffraction modes for the transmission gratings. The diffraction modes for both reflected and transmitted ones can be expressed as:

$$n_1\sin[\theta_r(m)] = n_1\sin\theta_i - \frac{\lambda_0}{\Lambda} \quad \text{(Reflection region)} \tag{2.1a}$$

$$n_2\sin[\theta_t(m)] = n_1\sin\theta_i - \frac{\lambda_0}{\Lambda} \quad \text{(Transmission region)} \tag{2.1b}$$

where $\theta_r(m)$ and $\theta_t(m)$ represent the angle of the mth order of the reflected and transmitted diffracted waves, respectively.

It is more convenient to study the diffraction mode in the $K-$space, where K refers to the wave number. We translate Equation 2.1 to wave vector expressions:

$$k_x(m) = \beta + m\frac{2\pi}{\Lambda} \quad m = 0, \pm1, \pm2, ... \tag{2.2}$$

Here $k_x(m)$ is the wave number for each diffraction mode along the grating groove direction, β is the wave number of the incident wave along the grating groove. Notice that in the k-space

the periodicity is along the grating groove direction. Taking the photonic crystal concept into account, the grating wave number will be

$$K = \frac{2\pi}{\Lambda} \tag{2.3}$$

The dispersion relation of the diffracted and incident wave will be periodic in K-space with periodicity of K.

Consider the incident wave number in the free space as k_0, and the diffraction modes can be categorized into propagating and evanescent modes. In order to achieve a propagating diffraction mode that carries energy, the order of the mode must satisfies $|k_x(m)| < \sqrt{\epsilon_s}|k_0|$, so that

$$-\sqrt{\epsilon_2}(1+\sin\theta_i)\frac{\Lambda}{\lambda} < m < \sqrt{\epsilon_2}(1-\sin\theta_i)\frac{\Lambda}{\lambda} \tag{2.4}$$

where ϵ_2 is the permittivity of the substrate.

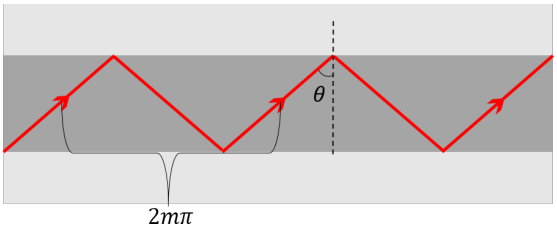

Figure 4: Schematics of ray picture of a waveguide mode property.

The guided mode resonance is a phenomenon such that the diffraction mode is also the eigenmode inside the waveguide (36). One can analyze it for both perpendicular and parallel polarization rigorously using time harmonic Maxwell's equations — Appendix Equation A.1 and boundary conditions:

$$\mathbf{D_1} \cdot \hat{\mathbf{n}} - \mathbf{D_2} \cdot \hat{\mathbf{n}} = \rho_s \tag{2.5a}$$

$$\hat{\mathbf{n}} \times \mathbf{E_1} - \hat{\mathbf{n}} \times \mathbf{E_2} = 0 \tag{2.5b}$$

$$\mathbf{B_1} \cdot \hat{\mathbf{n}} - \mathbf{B_2} \cdot \hat{\mathbf{n}} = 0 \tag{2.5c}$$

$$\hat{\mathbf{n}} \times (\mathbf{H_1} - \mathbf{H_2}) = \mathbf{J_s} \tag{2.5d}$$

By enforcing the boundary condition at two sides of the waveguide, we can obtain the eigenmodes of the waveguide. On the other hand, recalling that the Fresnel equations are derived based on the boundary conditions, and from Fresnel equations we can recover the reflection phase for the interface of the dielectric media from Equation 1.5. For the grating side, we can use the frequency domain computational EM method — Rigorous Coupled Wave Analysis(RCWA) (37) to achieve the reflection phase where the RCWA is introduced in the next section. In the geometric view which is shown in the Figure 4, a waveguide mode is formed when the light ray bounces back and forth inside the waveguide with the phase shift of a round trip as integer multiple of 2π

$$2k_0 n_c h \cos\theta - \sum_{n=1,2} \phi_n = 2m\pi \quad m = 0, 1, 2, ... \tag{2.6}$$

where k_0 is the free space wavenumber, n_c is the refractive index of the waveguide, h is the height of the waveguide, θ is the beam angle, and ϕ_n is the reflection phase at the interface of the waveguide for both TE and TM waves.

2.2.2 Guided mode resonance (GMR)

If the grating mode and waveguide were brought to proximity, and the diffraction mode matches with the waveguide mode, the external wave can be coupled to the waveguide mode. This phenomenon is denoted as guided mode resonance (GMR). Due to reciprocity, the waveguide mode can leak back out of the waveguide. Such guided modes are also called "*leaky modes*" since the guided modes are not completely confined while leaking energy out during propagation. The concept is very similar to the grating coupler for which the grating is used to couple the external light to the waveguide. For guided mode resonance, the structure can be simplified when the dielectric grating serves as grating but also the waveguide, which is also called grating waveguide structure. An example of guided mode resonance for dielectric grating is shown in Figure 5. A plane wave with "s" polarzation (E field out of plane) is normally incident on a dielectric grating made of Si and SiO_2 from the top which the grating is surrounded by free space. The color plot (color online) is the electric field distribution. In Figure.5a, the frequency is set off from the resonance, therefore the structure exhibits the normal response of transmission and reflection of a plane wave towards a dielectric slab. The structure at resonance is shown in Figure. 5b, where part of the applied wave is coupled into the counter propagating guided mode inside the grating. Notice that the electric field in the grating structure at resonance (shown in Figure. 5b) is much more enhanced. The guided mode then interferes with the incidence wave.

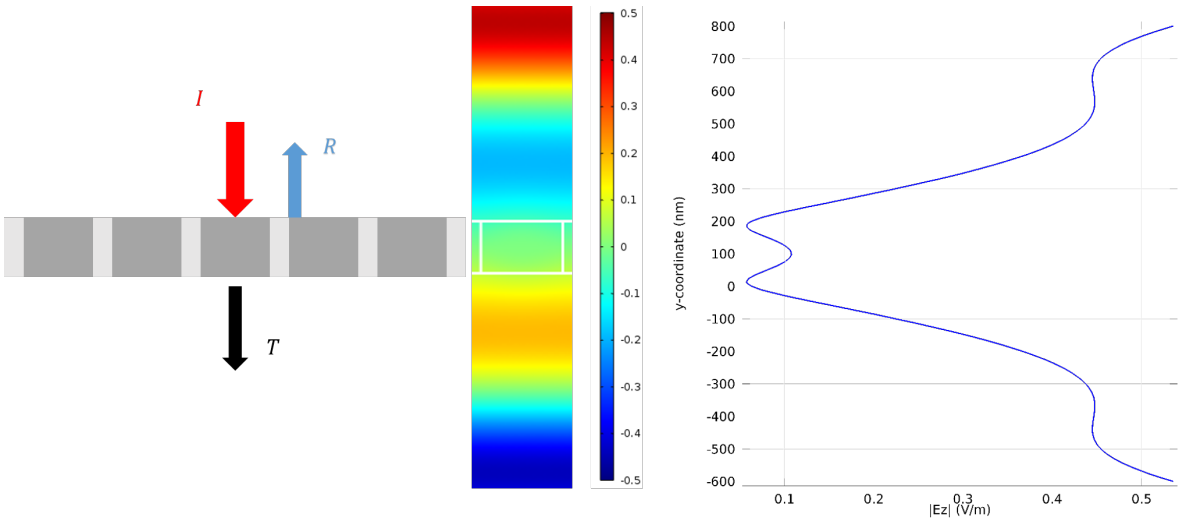

(a)

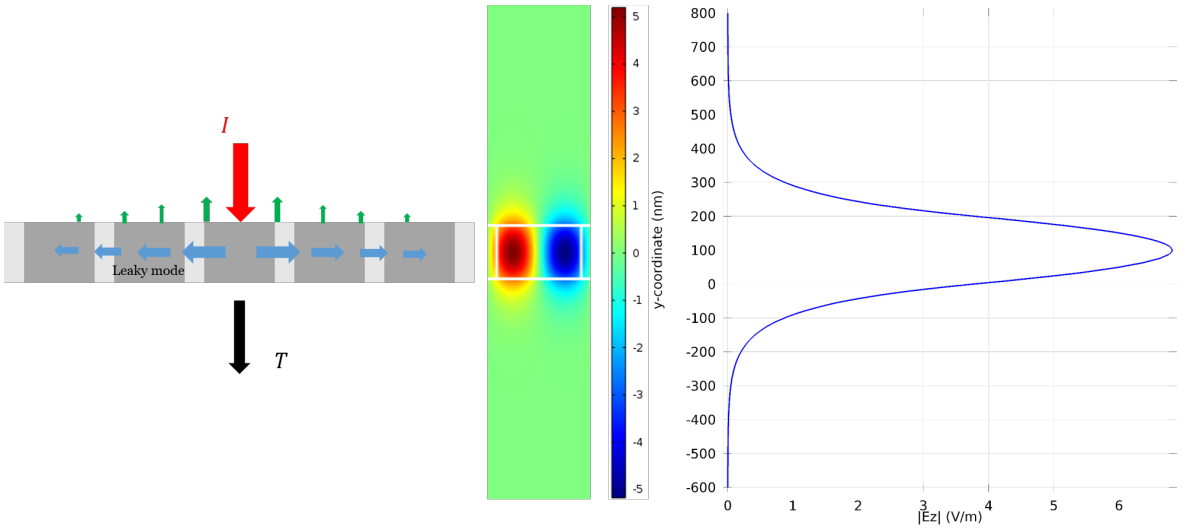

(b)

Figure 5: The schematics of normal incidence light to a SiO_2/Si grating with thickness 100 nm and the electric field distribution of one period of the grating. Fig. (a): shows the incidence, reflection and transmission wave when the frequency is off the guided mode resonance. The magnitude of electric field is shown right to the color plot. Fig. (b): shows the guided mode resonance case for which two counter propagating leaky modes are excited inside the dielectric grating.

If the leaky modes are in phase with the incident light (constructive interference), the grating functions as a high reflective mirror. If the leaky mode are 180° out of phase with the incidence (destructive interference), it is transparent to the light and can be a bandpass filter.

2.3 Characteristic field in periodic structure

The characteristic fields in a periodic structure is complicated. Since the environment is inhomogeneous, the usual Helmholtz equation is not applicable, but the field can be computed with FDTD (Finite-Difference-Time-Domain) (38) or FEM (Finite-Element-Method) (39) simulations using commercial and open source software. We implement the RCWA (Rigorous Coupled Wave Analysis) also called FFM (Fourier Modal Method) to fast and accurate compute the field components.

2.3.1 Guided mode in periodic structure

For a guided mode propagation along periodic waveguide, the plane wave approximation is not valid due to the nonuniform structure. Hence, a rigorous approach was introduced by Peng et al (40) to analyze the field inside the grating. A classic periodic thin-film structure is depicted in Figure 3, which shows a structure consisting of air, grating layer and substrate. The grating can be considered as a planar layer of constant thickness t_g whose composition varies periodically along x with period of Λ. Note that in the figure the permittivity $\epsilon(x)$ varies as a step function, however in general, it could be sinusoidal or of any other periodic forms.

Figure 6: Schematics for Fourier modal method analysis

2.3.1.1 Characteristic fields in the uniform regions

Assume a 1D structure shown in **??**. In a homogeneous media, according to the Helmholtz equation Equation A.7 the electric/magnetic (E/H) field can be written as

$$G(x,z) = G_0 \exp[j(k_x x + k_z z)] \tag{2.7}$$

Here G stands for either E or H field while G_0 is a constant and

$$k_x^2 + k_z^2 = k^2 = k_0^2 \epsilon \tag{2.8}$$

Here $k_0 = 2\pi/\lambda_0$ is the plane-wave propagation constant in free space and $\epsilon = n^2$ is the permittivity of the material. If the media is lossless, uniform structure will support waves that propagate without attenuation. These waves are therefore characterized by real values of $k_x = \beta$.

When a grating is superimposed on the uniform media, the electromagnetic wave should be modified to satisfy the periodic boundary conditions on the grating. Multiple modes are excited

due to the diffraction caused by the grating (41). Modes in uniform regions must appear in the Floquet form

$$G(x,z) = \sum_n G_n \exp[j(k_{xn}x + k_{zn}z)] \tag{2.9}$$

Note that this form applies to all uniform regions except for the grating region. Here we have to introduce the Floquet period boundary condition. The Floquet theorem (42) is commonly known as Bloch's theorem (43) in solid-state physics and requires that the field satisfies the following condition in the K space

$$G(k_x) = G(k_x + m\frac{2\pi}{\Lambda}) \quad (m = 0, \pm1, \pm2, ...) \tag{2.10}$$

if periodicity occurs along the x direction, where n is integer. Hence, values of the wavenumber k_x that differ by integral multiples of $2\pi/\Lambda$ are not different from a physical point of view. Thus, the mode frequencies must also be periodic in k_x: $\omega(k_x) = \omega(k_x + 2n\pi/\Lambda)$. Therefore, we will only need to consider k_x exist in the range $-\pi/\Lambda < k_x \leq \pi/\Lambda$. This important region with nonredundant values of k_x is call the Brillouin zone.

The quantities k_{xn} are related to the fundamental longitudinal factor k_{x0} by the Floquet condition:

$$k_{xn} = k_{x0} + 2n\pi/d \quad (n = 0, \pm1, \pm2, ...) \tag{2.11}$$

Each partial function $G_n \exp[j(k_{xn}x + k_{zn}z)]$ of $G(x, z)$ exists in a uniform region and must satisfy the Helmholtz equation, Equation 2.7, leading to the dispersion relation:

$$k_{zn} = \pm\sqrt{k^2 - k_{xn}^2} \tag{2.12}$$

Observe that each nth partial function can be regarded as a mode with transverse variation $\exp(jk_{xn}x)$ along x, which propagated along z with a propagation factor k_{zn}. Hence, within a finite-thickness layer, both signs in Equation 2.12 shall be counted because they refer to waves that travel along both $+z$ and $-z$ directions, respectively. Thus, each nth term in Equation 2.10 includes two separate components. On the other hand, in the open regions, it is necessary to restrain the component so the energy decays or flows when travel away from the structure.

The propagation constant of the 0th order mode k_{x0} would be very close to the propagation factor k_x of the incidence wave if the grating's diffraction efficiency is small (no gratings present). And in general, higher order modes possess very small amount of energy. However, some of these higher order modes may modify the nature of the guided wave, therefore, all higher modes must be accounted for to satisfy the boundary conditions.

The following feature may be clarified by considering a plane wave incident from the left in a homogeneous media, as shown in Figure 3. Assuming the grating is long enough to be treated as infinite along x direction. The traveling wave will leak into the medium on the other side of the grating by adding up the scattering at a large portion of the energy brought into the grating region by the incident wave. The individually scattered waves interfere constructively

only along certain preferred directions. Because energy loss occurs due to radiation, the total guided field must decay with x as it propagates along the grating region. Hence, the propagation factor k_{x0} along the grating region cannot remain purely real, but, instead, k_{x0} is changed from the incidence's propagation constant β to complex values:

$$k_{xn} = \beta_n + j\alpha_n = \left(\beta_0 + \frac{2n\pi}{\Lambda}\right) + j\alpha \tag{2.13}$$

where the imaginary term $\alpha > 0$ is responsible for the decay due to leakage. Notice that the longitudinal decay factor α is the same for all the partial field components in Equation 2.9, which is constrained by the Floquet theory. The wave number k_{zn} is then complex as well according to Equation 2.8.

$$k_{zn} = \xi_n + j\eta_n \tag{2.14}$$

However, different from k_{xn}, the imaginary part of k_{zn} is generally different for each mode. Because k_{zn} is given by $k_{zn} = \sqrt{k_0^2 - k_{xn}^2}$. This leaves the question about sign should be used in evaluating k_{zn}, i.e. the propagating constant for upward propagation. The signs of components in k_{zn} are selected according to

$$\eta_n \beta_n > 0 \tag{2.15}$$

because waves guided by periodic structures generally contain radiating field components, which are called leaky waves. The sign selection in Equation 2.15 then satisfies the energy conservation law.

2.3.1.2 Characteristic fields in the grating regions

To evaluate the fields supported by the grating layer, we have to analyze the wave specifically for two orthogonal polarizations. The Helmholtz equation will then be written as:

$$\nabla^2 G_{grt} + k^2(x) G_{grt} = 0 \tag{2.16}$$

where G_{grt} refers to the E or H fields and $k^2(x) = \epsilon(x) k_0^2$. Note that the wavenumber is not a constant but varies with x since the permitivitty of the media is defined as $\epsilon(x)$.

Since $\epsilon(x)$ is periodic, we can then represent $k(x)$ with a Fourier series. First, we can expand the permitivitty function $\epsilon(x)$ into Fourier coefficients ϵ_n by Fourier transform:

$$\varepsilon_n = \frac{1}{\Lambda} \int_0^{\Lambda} \epsilon(x) \times \exp(-jnKx) dx \tag{2.17}$$

where $K = 2\pi/\Lambda$. We may then have:

$$G_{grt} = \sum_n G_n(z) \exp(jk_{xn}x) \tag{2.18}$$

where G_n stands for the nth order coefficient for either E or H field.

For TE polarization the possible field components are (E_y, H_x, H_z) and we have

$$E_y = \sum_n \mathcal{E}_{yn}(z) \exp(-jk_{xn}x) \tag{2.19a}$$

$$H_x = -j\sqrt{\frac{\epsilon_0}{\mu_0}} \sum_n \mathcal{H}_{xn}(z) \exp(-jk_{xn}x) \tag{2.19b}$$

Here $\mathcal{E}_{yn}(z)$ and $\mathcal{H}_{xn}(z)$ are the field components of nth order. H_z is not shown since we only care for transverse components. According to Maxwell's equation, we find:

$$\frac{\partial E_y}{\partial z} = j\omega\mu_0 H_x \tag{2.20a}$$

$$\frac{\partial H_x}{\partial z} = j\omega\epsilon_0\epsilon(x)E_y + \frac{\partial H_z}{\partial x} \tag{2.20b}$$

$$\frac{\partial^2 E_y}{\partial z^2} = -j\omega\epsilon_0\mu_0\epsilon(x)E_y \tag{2.20c}$$

Substituting Equation 2.19a and Equation 2.19b into Equation 2.20a and Equation 2.20b and eliminating H_z, we obtain the coupled-wave equations:

$$\frac{\partial \mathcal{E}_{yn}}{\partial z} = k_0 \mathcal{H}_{xn} \tag{2.21a}$$

$$\frac{\partial \mathcal{H}_{xn}}{\partial z} = \left(\frac{k_{xn}}{k_0}\right)^2 \mathcal{E}_{yn} - k_0 \sum_m \varepsilon_{n-m}\mathcal{E}_{ym} \tag{2.21b}$$

Here n and m are integers.

In matrix form,

$$\begin{bmatrix} \frac{\partial E_y}{\partial z} \\ \\ \frac{\partial H_x}{\partial z} \end{bmatrix} = j\omega \begin{bmatrix} 0 & I \\ \\ \mathbf{K}^2 - [\epsilon] & 0 \end{bmatrix} \begin{bmatrix} E_y \\ \\ H_x \end{bmatrix} \tag{2.22}$$

which may be reduced to,

$$\left[\frac{\partial^2 E_y}{\partial z^2}\right] = j\omega\Big[\mathbf{K}^2 - [\epsilon]\Big]\Big[E_y\Big] \tag{2.23}$$

where $[\epsilon]$ is the matrix formed by the permittivity coefficient with m, n element being ε_{m-n}, $\mathbf{K}$ is a diagonal matrix with the n, n entry being k_n/k_0, I is an identity matrix. Here E_y and H_x components are both matrices.

For TM polarization the possible field components are (H_y, E_x, E_z) and we have

$$\frac{\partial H_y}{\partial z} = j\omega\epsilon(x)E_x \tag{2.24a}$$

$$\frac{\partial E_x}{\partial z} = j\omega\mu_0 H_y + \frac{1}{k_0}\frac{\partial}{\partial x}\left(\frac{1}{\epsilon(x)}\frac{\partial H_z}{\partial x}\right) \tag{2.24b}$$

$$\frac{\partial^2 H_y}{\partial z^2} = \epsilon(x)\left[\frac{\partial}{\partial x}\left(\frac{1}{\epsilon(x)}\frac{\partial H_y}{\partial x}\right) + \mu_0 k_0^2 H_y\right] \tag{2.24c}$$

Using the same method, we find:

$$\frac{\partial \mathcal{H}_{yn}}{\partial z} = jk_0 \sum_m \varepsilon_{n-m}\mathcal{E}_{xm} \tag{2.25a}$$

$$\frac{\partial \mathcal{E}_{xn}}{\partial z} = jk_0\mu_0\mathcal{H}_{yn} - \frac{k_n}{k_0}\sum_m \left(\frac{1}{\varepsilon_{n-m}}\right) k_m \mathcal{H}_{ym} \tag{2.25b}$$

However, in Equation 2.25a, $\partial\mathcal{H}_{yn}/\partial z$ is the derivative of uniformly convergent Fourier series. However, the right-hand side is a non-uniformly convergent trigonometric series. These

two series does not converge in the same rate and neither match in corresponding order. The continuity of $\epsilon(x)E_x$ cannot be preserved uniformly. We use the Toeplitz matrix $[\epsilon]$ to preserve the continuity (44).

$$\frac{\partial \mathcal{H}_{yn}}{\partial z} = jk_0 \sum_m \left[\frac{1}{\epsilon}\right]^{-1}_{nm} \mathcal{E}_{xm} \tag{2.26a}$$

$$\frac{\partial \mathcal{E}_{xn}}{\partial z} = jk_0\mu_0 \mathcal{H}_{yn} - \frac{k_n}{k_0} \sum_m [\epsilon]^{-1}_{nm} k_m \mathcal{H}_{ym} \tag{2.26b}$$

We have:

$$\frac{\partial^2 E_{xn}}{\partial z^2} = \sum_m (k_{xn}[\epsilon]^{-1}_{nm} k_{xm} - \mu_0 k_0^2 \delta_{nm}) \sum_l \left[\frac{1}{\epsilon}\right]^{-1}_{ml} E_{xn} \tag{2.27}$$

Same as TE polarization, this leads to an eigen value problem which will be deliberately discussed in next section rigorous coupled wave analysis.

2.4 Rigorous Coupled Wave Analysis (RCWA)

Rigorous coupled wave analysis, or Fourier Modal Method, is introduced to compute Electromagnetic field in 2D periodic structures with periods Λ_x and Λ_y (40; 37). The 1D binary grating will then be considered as a special case for 2D strictures with $\Lambda_y = 0/\infty$. For 2D structures, polarizations will introduce EM symmetry which can greatly reduce the computation load. The transverse and longitudinal view of the multilayer 2D structures that RCWA treats is shown in Figure 7. The field inside each layer is represented as the summation of positive and negative propagating eigenmodes $[\mathrm{VE}]u^{(p)}$ and $[\mathrm{VE}]d^{(p)}$, respectively. Here VE or VH stand for eigenmodes of transverse E and H fields. $u^{(p)}$ and $d^{(p)}$ are both vectors with each element, the coefficient of the corresponding eigenmode, p stands for the order of the layer.

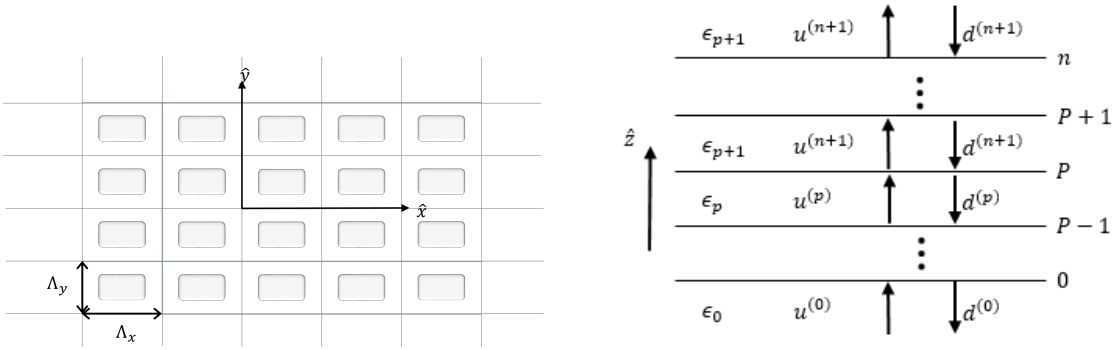

(a) (b)

Figure 7: Structure of a multilayer grating and the representation of fields inside each layer. (a): Transverse view, (b): Longitudinal view.

2.4.1 Eigenvalue Problem

In RCWA (37), for each layer that is invariant in the $\hat{z}$ direction while 2D periodic in the $\hat{x} - \hat{y}$ directions, the eigenmode is assumed to be:

$$\mathbf{E}^{(p)} = \mathbf{E}_p(x, y)e^{jk_z^{(p)}z} \tag{2.28a}$$

$$\mathbf{H}^{(p)} = \mathbf{H}_p(x, y)e^{jk_z^{(p)}z} \tag{2.28b}$$

where p indicates the p^{th} layer. $k_z^{(p)}$ is the propagating constant along $\hat{z}$. Notice that $\mathbf{E}_p$ and $\mathbf{H}_p$ both have three component ($\hat{x}$, $\hat{y}$ and $\hat{z}$). However, since matching the boundary conditions would need only the transverse components, only those in xy plane will be considered. The longitudinal component ($\hat{z}$) can then be recovered from those components using Equation 2.30. The eigenproblem is also constructed for the transverse components only.

From time harmonic Maxwell's equation, we find:

$$\nabla \times \mathbf{E} = j\omega\mu\mathbf{H} \tag{2.29a}$$

$$\nabla \times \mathbf{H} = j\omega\epsilon\mathbf{E} \tag{2.29b}$$

In Cartesian coordinates,we find:

$$j\omega\mu H_z = \frac{\partial E_y}{\partial x} - \frac{\partial E_x}{\partial y} \qquad -j\omega\epsilon E_z = \frac{\partial H_y}{\partial x} - \frac{\partial H_x}{\partial y} \tag{2.30a}$$

$$j\omega\mu H_x = \frac{\partial E_z}{\partial y} - \frac{\partial E_z}{\partial z} \qquad -j\omega\epsilon E_x = \frac{\partial H_z}{\partial y} - \frac{\partial H_y}{\partial z} \tag{2.30b}$$

$$j\omega\mu H_y = \frac{\partial E_x}{\partial z} - \frac{\partial E_y}{\partial x} \qquad -j\omega\epsilon E_y = \frac{\partial H_x}{\partial z} - \frac{\partial H_z}{\partial x} \tag{2.30c}$$

Using the equations above, we can transform the partial differential equation into a eigenvalue problem. Consider z as the wave propagation direction, by analyzing the transverse electrical field $E_T(x, y)e^{jk_z z}$ in x, y direction, we can have other entire field component information. Here E_T refers to the transverse field. By substituting equations into each other from the equation set Equation 2.30 we show:

$$\frac{\partial E_x}{\partial z} = \left(j\omega\mu + \frac{j}{\omega\epsilon}\frac{\partial^2}{\partial x^2}\right) H_y - \frac{j}{\omega\epsilon}\frac{\partial^2}{\partial x \partial y} H_x \tag{2.31a}$$

$$\frac{\partial E_y}{\partial z} = -\left(j\omega\mu + \frac{j}{\omega\epsilon}\frac{\partial^2}{\partial y^2}\right) H_x + \frac{j}{\omega\epsilon}\frac{\partial^2}{\partial x \partial y} H_y \tag{2.31b}$$

$$\frac{\partial H_x}{\partial z} = -j\omega\epsilon H_y - \frac{j}{\omega\epsilon}\left(\frac{\partial^2}{\partial x^2} E_y - \frac{\partial^2}{\partial x \partial y} E_x\right) \tag{2.31c}$$

$$\frac{\partial H_y}{\partial z} = \left(j\omega\epsilon + \frac{j}{\omega\mu}\frac{\partial^2}{\partial y^2}\right) E_x - \frac{j}{\omega\mu}\frac{\partial^2}{\partial x \partial y} E_y \tag{2.31d}$$

Writing Equation 2.31d into matrix form, yields

$$\frac{\partial}{\partial z}\begin{bmatrix} E_x \\ E_y \end{bmatrix} = \underbrace{\begin{bmatrix} -\frac{j}{\omega\epsilon}\frac{\partial^2}{\partial x \partial y} & -j\omega\mu - \frac{j}{\omega\epsilon}\frac{\partial^2}{\partial x^2} \\ -j\omega\mu - \frac{j}{\omega\epsilon}\frac{\partial^2}{\partial y^2} & \frac{j}{\omega\epsilon}\frac{\partial^2}{\partial x \partial y} \end{bmatrix}}_{\mathbf{F}} \begin{bmatrix} H_x \\ H_y \end{bmatrix} \tag{2.32a}$$

$$\frac{\partial}{\partial z}\begin{bmatrix} H_x \\ H_y \end{bmatrix} = \underbrace{\begin{bmatrix} \frac{j}{\omega\mu}\frac{\partial^2}{\partial x \partial y} & -j\omega\epsilon - \frac{j}{\omega\mu}\frac{\partial^2}{\partial x^2} \\ j\omega\mu + \frac{j}{\omega\mu}\frac{\partial^2}{\partial y^2} & -\frac{j}{\mu\epsilon}\frac{\partial^2}{\partial x \partial y} \end{bmatrix}}_{\mathbf{G}} \begin{bmatrix} E_x \\ E_y \end{bmatrix} \tag{2.32b}$$

Let **F** and **G** represent the matrices described in the equations above, we can have:

$$\left.\begin{aligned} \frac{\partial^2}{\partial z^2}\begin{bmatrix} E_x \\ E_y \end{bmatrix} &= \mathbf{FG}\begin{bmatrix} E_x \\ E_y \end{bmatrix} \\ \frac{\partial^2}{\partial z^2}\begin{bmatrix} E_x \\ E_y \end{bmatrix} &= -k_z^2\begin{bmatrix} E_x \\ E_y \end{bmatrix} \end{aligned}\right\} \Longrightarrow \left(\mathbf{FG} + k_z^2\right)\begin{bmatrix} E_x \\ E_y \end{bmatrix} = 0 \tag{2.33}$$

2.4.2 Fourier Modes

For each layer the electromagnetic field can be expanded in Floquet-Fourier series (42),

$$\Psi(x, y, z) = \sum_{m,n}(z)\exp(jk_{xm}x + jk_{yn}y) \tag{2.34}$$

$$k_{xm} = k_{x0} + \frac{2m\pi}{\Lambda_x}$$

$$k_{yn} = k_{y0} + \frac{2n\pi}{\Lambda_y}$$

where Φ stands for any one of the E/H field components. For a homogeneous layer, where ϵ is a constant, which can be directed solved for the eigen vectors using For the grating layer, the z-dependent Fourier coefficients Ψ_{mn} are to be solve from Eq. (32)-(34) of Ref. (37).

Since the transverse fields are represented in Fourier components, the number of those components are infinite. For computational purposes, we select the highest order Fourier component in the $\hat{x}$ and $\hat{y}$ direction and refer to them as M_1 and M_2, respectively. That means for each direction, we have $2M_i + 1$ components from $-M_i$ to M_i. The field are represented by their Fourier components by $\mathbf{e}$ for E field and $\mathbf{h}$ for H field. Each field vector has two parts, the x component and the y component, i.e.:

$$\mathbf{e} = \begin{bmatrix} \mathbf{e}_x \\ \\ \mathbf{e}_y \end{bmatrix}; \quad \mathbf{h} = \begin{bmatrix} \mathbf{h}_x \\ \\ \mathbf{h}_y \end{bmatrix} \tag{2.35}$$

The mode indexing $\mathbf{e}_{x,y}$ and $\mathbf{h}_{x,y}$ are one-dimensional while the Fourier modes have components in two directions. A rule to map spatial Fourier components of order (m, n) with m the order for that of $\hat{x}$ direction while n for that of $\hat{y}$ direction to the linear index of the elements of $\mathbf{e}_{x,y}$ and $\mathbf{h}_{x,y}$ is needed. The resulting map is:

$$\begin{aligned}[(-M_1, -M_2), (-M_1, -M_2 + 1), ..., (-M_1, M_2 - 1), (-M_1, M_2), ... \\ (-M_1 + 1, -M_2), (-M_1 + 1, -M_2 + 1), ..., (M_1, M_2 - 1), (M_1, M_2)]^T\end{aligned} \tag{2.36}$$

We can solve the eigenproblem solely for **e** vectors, while **h** vector can be obtained from **e** afterwards. The size of **e** would be $M = 2(2M_1 + 1)(2M_2 + 1)$, which is also the rank of the eigenproblem. The eigenproblem will give M eigenvectors and the same number of eigenvalues. All the eigenvectors when placed side by side form a eigenvector matrix **VE**,

$$\mathbf{VE} = [\mathbf{e}_1, \mathbf{e}_2, ..., \mathbf{e}_M] \tag{2.37}$$

The corresponding k_z should form a vector **D**,

$$\mathbf{D} = [k_z|_1, k_z|_2, ..., k_z|_M]^T \tag{2.38}$$

The corresponding **h** vectors form matrix of **VH**,

$$\mathbf{VH} = [\mathbf{h}_1, \mathbf{h}_2, ..., \mathbf{h}_M] \tag{2.39}$$

2.4.3 Field inside each layer

After the eigenproblem for each layer is solved, the transverse components of the fields in layer p is represented by the positive and negative propagating eigenmodes as:

$$\begin{bmatrix} \mathbf{E}_T^{(p)}(x,y,z) \\ \mathbf{H}_T^{(p)}(x,y,z) \end{bmatrix} = \begin{bmatrix} \mathbf{VE}^{(p)} \\ \mathbf{VH}^{(p)} \end{bmatrix} \begin{bmatrix} e^{jk_z^{(p)}|_1 z} & 0 & \cdots & 0 \\ 0 & e^{jk_z^{(p)}|_2 z} & \cdots & 0 \\ \vdots & \vdots & \ddots & \vdots \\ 0 & \cdots & \cdots & e^{jk_z^{(p)}|_M z} \end{bmatrix} u^{(p)} + \begin{bmatrix} \mathbf{VE}^{(p)} \\ \mathbf{-VH}^{(p)} \end{bmatrix} \begin{bmatrix} e^{-jk_z^{(p)}|_1 z} & 0 & \cdots & 0 \\ 0 & e^{-jk_z^{(p)}|_2 z} & \cdots & 0 \\ \vdots & \vdots & \ddots & \vdots \\ 0 & \cdots & \cdots & e^{-jk_z^{(p)}|_M z} \end{bmatrix} d^{(p)} \tag{2.40}$$

Here $u^{(p)}$ and $d^{(p)}$ stand for the coefficients of each up/down propagation eigenmode. Notice that the eigenmodes for down propagation is the same as the that for up propagation only that the matrix for H field is of the negative sign. The length of $u^{(p)}$ and $d^{(p)}$ is the same as the rank of **VE**, which is M. The origin of z used for each layer is the bottom boundary of that layer. This means $u^{(p)}$ and $d^{(p)}$ are actually the coefficients of each eigenmode of the corresponding layer at the lower boundary.

Let

$$\mathbf{W}^{(p)} = \begin{bmatrix} \mathbf{VE}^{(p)} & \mathbf{VE}^{(p)} \\ \mathbf{VH}^{(p)} & -\mathbf{VH}^{(p)} \end{bmatrix} \tag{2.41}$$

We then have

$$\begin{bmatrix} \mathbf{E}_T^{(p)}(x,y,z) \\ \mathbf{H}_T^{(p)}(x,y,z) \end{bmatrix} = \mathbf{W}^{(p)} \begin{bmatrix} \exp(jk_z|_m z) & 0 \\ 0 & \exp(-jk_z|_m z) \end{bmatrix} \begin{bmatrix} u^{(p)} \\ d^{(p)} \end{bmatrix} \tag{2.42}$$

The entire field components can be revealed by the transverse field described in Equation 2.42. Note that the longitudinal field can be obtained by time harmonic Maxwell's equations (Equation 2.30). Also, due to the orthogonality in Fourier space, the Fourier modes for each layer have one to one correspondence to match the boundary condition (the modes with identical spatial frequency). By matching the amplitude of the mode coefficient $u^{(p)}$ and $d^{(p)}$, the field characteristics can be revealed for every single layer.

Besides RCWA (37), Finite Element Methods (FEM) (39) and FDTD (Finite Different Time Domain method) (38) can be applied to solve a 2D periodic structure problem. However, they suffer from trade-off between computational efficiency (size of mesh grid) and accuracy. RCWA is considered a fast and accurate method to analysis periodic structure and guided mode resonance.

CHAPTER 3

GIANT POSITIVE AND NEGATIVE GOOS-HÄNCHEN SHIFT BASED ON GUIDED MODE RESONANCE

***Disclaimer**: This chapter is reproduced from published paper — Rui Yang, Wenkan Zhu, Jingjing Li, "Giant positive and negative Goos-Hänchen shift based on guided mode resonance", Opt. Express 22, 2043-2050 (2014). The author of this thesis was the main contributor to the publication.*

In this chapter, giant positive and negative Goos-Hänchen shifts of more than 5000 times of the operating wavelength are observed when a beam is totally reflected from a substrate covered by a dielectric grating. Different from the former studies for which Goos-Hänchen shift is related to metamaterials or plasmonic materials with ohmic loss, here the giant shift is realized with 100% reflectance without the loss. This is extremely advantageous for sensor applications due to achievable high signal to noise ratio. The Goos-Hänchen shift exhibits a strong resonant feature at the frequency of guided mode resonance, and is associated to the energy flow carried by the guided mode.

3.1 Schematics and Dispersion Property of Periodic Dielectric Grating

The structure we considered is a binary 1D grating of thickness t, period Λ and filling factor F sitting on a dielectric substrate, as shown in Figure 8. The filling factor is defined as the ratio of the width of high refractive index part to the period, i.e. $F = a/\Lambda$. The grating consists of

two parts having relative permittivity of ϵ_h and ϵ_l ($\epsilon_h > \epsilon_l$). In general, the lower permittivity part is considered to be the same as the environment. The substrate is of permittivity ϵ_s and the environment that of ϵ_c, respectively.

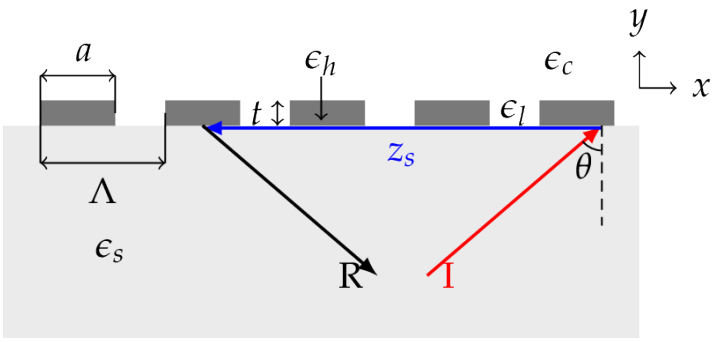

Figure 8: Schematic of a dielectric gating and the Goos-Hänchen shift under total internal reflection. The grating has a spatial period Λ, a is the length of the portion of the grating with high refractive index ϵ_h and $F = a/\Lambda$ is the filling factor. "I" and "R" refer to the incident and reflected beams respectively. z_s is the Goos-Hänchen shift.

The dispersion property of the eigenmodes propagating towards the lateral $+\hat{x}$ direction is studied. Figure 9 shows the dispersion curve of a grating of $\Lambda = 0.43\mu$m, $t = 0.11\mu$m, $\epsilon_h = 12.12$(Si), $\epsilon_l = \epsilon_c = 1$. Notice that the wave numbers depicted in this thesis are all normalized to $K = 2\pi/\Lambda$, which is the periodicity of the grating's reciprocal lattice. To achieve the dispersion property, software package MEEP(MIT Electromagnetic Equation Propagation), a numerical electromagnetic solver based on the finite-difference time-domain algorithm is used

(38). Both s (electric field perpendicular to xy plane)and p (electric field parallel to xy plane) polarized modes are studied (referring to Figure 8).

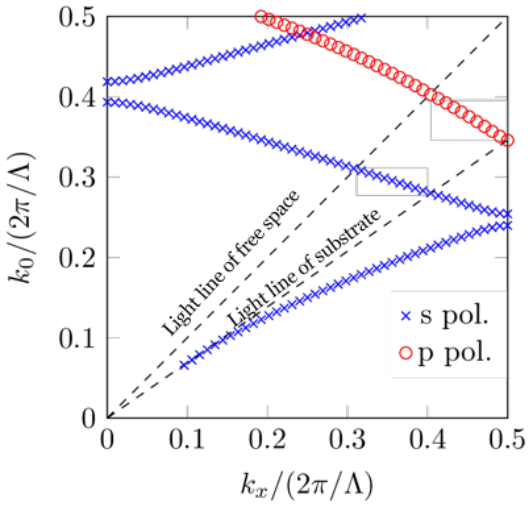

Figure 9: Dispersion curve for guided mode of "s" and "p" polarizations. The grating's parameters are: $\Lambda = 0.43\mu$m, $t = 0.11\mu$m, $\epsilon_h = 12.12$ (Si), $\epsilon_l = \epsilon_c = 1$ (free space), $\epsilon_s = 2.09$ (SiO_2). The top dashed line is the light line of the free space while the bottom one is the light line of the substrate. The grey boxes shows the guided mode of the grating between the two light lines.

Figure 8 shows typical dispersion features of a periodic crystalline structure. Here k_0 represents the wave number of the free space while k_x stands for the lateral wave number in the x direction. According to Floquet theory for periodic structures, the entire dispersion property is shown in the first Brillouin zone, which corresponds to the k_x values in the range [0, π/Λ] in Figure 9. For the s (perpendicular) polarization, the lowest band is below the light line of

the substrate, thus is confined to the grating structure without any coupling to the substrate or propagating components. This band represent a conventional positive propagating guided mode (i.e. the energy flow is at the same direction of the wave vector k_x). A typical band gap of photonic crystal shows up at the edge of the first Brillouin zone, above which lies the second band that is a negative propagating mode (energy flows towards $-\hat{x}$ direction). Recalling that the speed of energy flow or the group velocity is

$$v_g = \frac{\partial \omega}{\partial k_x} = \frac{1}{c}\frac{\partial k_0}{\partial k_x} \tag{3.1}$$

where c is the speed of light inside the grating. The lower part of this band is still below the light line of the substrate, and is a confined, negative flowing guided mode. As the operating frequency k_0 increases, the mode goes above the light line of the substrate when it begins to leak energy into the substrate, and finally above the free space light line when the mode leaks to both sides. In former studies of guided mode resonance for reflector and filter applications, it was usually the part above the free space light line that was used, which cannot sustain total reflection. Since the Goos-Hänchen shift studied in this thesis focuses on total internal reflection, the specific interest resides in the part between the two light lines when propagating incidence from the substrate is used (refer to the grey boxes in Figure 9).

3.2 Reflection Property and Goos-Hänchen Shift of the Grating Based On Guided Mode Resonance

According to Artmman's theory (2), large Goos-Hänchen shift occurs only with a very sharp change of reflection phase loss with little incident angle variation. Our study finds an abnormal reflection phase loss compared to what would be expected from general total internal reflection property, which leads to a very large negative Goos-Hänchen shift. A detailed study shows that the guided mode resonance inside the grating is responsible for the large Goos-Hänchen shift and will be discussed next.

3.2.1 Abnormal Reflection Phase and Giant Negative Goos-Hänchen Shift

The guided modes of the grating between the two line lights (refer to grey boxes in Figure 9) are the total internal reflection region. The reflection property for a plane wave incident from the substrate for various angles (i.e. various k_x) is studied. Since the properties of s and p polarizations are similar, only the result of s polarization is explicitly discussed. k_0 and k_x are selected so that inside the substrate only the 0th order diffraction (the direct reflection) propagates, while all higher order diffraction modes are evanescent, corresponding to

$$\left| k_x - \frac{2\pi}{\Lambda} \right| < k_0 \tag{3.2}$$

The free space wavelength of the incidence is 1.5μm, corresponding to $k_0/(2\pi/\Lambda) = 0.287$. Rigorous coupled wave analysis (RCWA) (37)was used to compute the reflection coefficient for k_x between the two light lines ($0.287 \sim 0.414 \times 2\pi/\Lambda$, or $43.8^\circ < \theta_i < 90^\circ$). The resulting phase

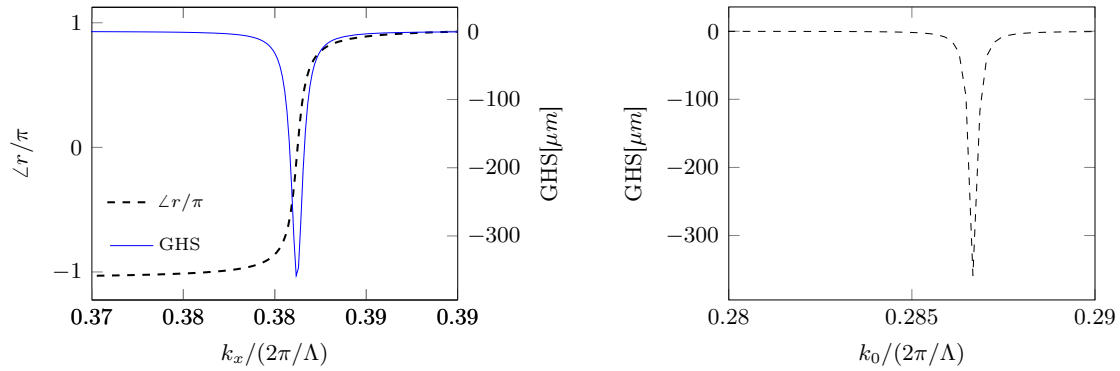

Figure 10: (a): Reflection phase loss $\angle r$ (dashed line) and Goos-Hänchen shift (solid line) vs normalized k_x for a incidence of $1.5\mu m$ free space wavelength from the substrate. (b): Goos-Hänchen shift vs normalized k_0 for an incidence from the substrate side with $k_x = 0.38 \times 2\pi/\Lambda$. The k_x corresponds to the maximum dip of the Goos-Hänchen shift in (a). The k_0, where the Goos-Hänchen shift's magnitude is maximum corresponds to the guided mode resonance frequency of the k_x value.

is shown in 10a with a dashed line. Notice that the magnitude of the reflection coefficient remains 1 throughout the whole k_x range because $k_0 < k_x < \sqrt{\epsilon_s}k_0$ which is the condition of total internal reflection. The curve of the reflection phase loss exhibits a sharp increase of almost 2π at k_x around $0.38 \times 2\pi/\Lambda$. This is exactly the value of k_x when the guided mode resonance at this frequency is excited, as confirmed by the point of $(k_0, k_x) = (0.287, 0.38)$ in Figure 9. Here k_0, k_x are normalized to $2\pi/\Lambda$. Hence, it is confirmed that the abnormal phase change at this k_x is caused by the guided mode resonance excited in the grating.

Recall from Artmman's theory that the Goos-Hänchen shift can be expressed by the derivative of the reflection phase loss to the lateral wavenumber k_x given in Equation 1.6. The drastic

increase of phase with k_x indicates a negative Goos-Hänchen shift of giant magnitude which is shown by the solid line in Figure 10a. At its maximum magnitude, the Goos-Hänchen shift reaches a value of 360μm, about 240 times the free space wavelength. The frequency dispersion of the Goos-Hänchen shift for incidence at a fixed k_x is also studied and is shown in Figure 10b, For $k_x = 0.38 \times 2\pi/\Lambda$ corresponding to when the Goos-Hänchen shift achieves its maximum magnitude in Figure 10a. Hence, the Goos-Hänchen shift exhibits an obvious resonance peak, and the resonant frequency corresponds to that of the guided mode resonance. Such a resonant property has wide applications for sensors as discussed in Chapter 2. It is necessary to point out that, in our design, the giant negative Goos-Hänchen shift is achieved when the magnitude of the reflection coefficient maintains 1 and with a much greater magnitude of Goos-Hänchen shift. This result is in sharp contrast of some former studies when large negative Goos-Hänchen shift is achieved at the cost of resonant ohmic loss with a reflectance towards 0 (45) . A large reflectance means better signal to noise ratio in sensor applications, thus is of great engineering importance.

3.2.2 Guided Mode Resonance

To explicitly reveal the relationship between the resonant behavior of Goos-Hänchen shift and the excitation of guided mode resonance, the field distribution and Poynting vector inside and outside the grating at the resonance of Goos-Hänchen shift are analyzed. The results are shown in Figure 11, where the color indicates the instantaneous distribution of electric field E_z. The result in Figure 11a is achieved for $\lambda_0 = 1.5\mu$m free space wavelength, $k_x = 0.38 \times 2\pi/\Lambda$ when Goos-Hänchen shift is of the negative value of maximum magnitude. Notice that the

incidence comes from the substrate ($y < 0$) from the lower left side. In the color plot, we notice a strong field around the grating is excited with a field strength much stronger than that of the incidence, which is identified as the guided mode of the grating. What is more interesting is the energy flow. The x component of the Poynting vector on a line parallel to $\hat{y}$ and through the center of a grating period (refer to the white dashed line in the color plot of Figure 11a) is plotted as a function of y and is placed next to the field plot. Notice that, around the grating ($0 < y < 0.11\mu m$), S_x shows a strong dip of negative value. Far away from the grating inside the substrate, the field is a plane wave that is standing along the y direction while propagating towards $+x$, thus a positive S_x is observed (see the inset of Figure 11a). However, the maximum magnitude of negative Sx inside the grating is about 500 times larger than the positive S_x $1\mu m$ away from the grating. This is consistent with the explanation of Goos-Hänchen shift in Ref.(15) where the negative Goos-Hänchen shift is attributed to the negative energy flow beyond the reflection interface. For comparison purposes, we also present the results at a condition far from the guided mode resonance when a mediocre positive Goos-Hänchen shift of $0.33\mu m$ is observed and shown in Figure 11b. As we can see, no obvious field enhancement inside the grating can be observed, and the energy still flows to the $+x$ direction inside the grating.

The relationship between the guided mode resonance and the giant Goos-Hänchen shift is most obviously seen in Figure 12a, where the Goos-Hänchen shift for k_0 and k_x in the range inside the grey box in Figure 9 is shown. In this plot, the color plots represent the Goos-Hänchen shift, while the crosses represent the eigenmodes on the dispersion curve inside the

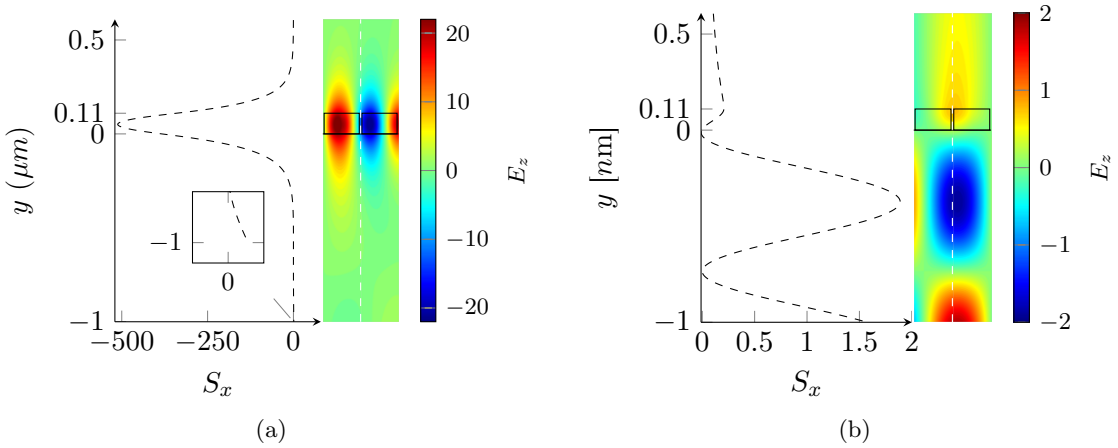

Figure 11: Instantaneous distribution of the electric field E_z (the color plot). The plot for the distribution of the x component of the Poynting vector (S_x) along the white dashed line is placed nearby. The operating conditions are the same as inFigure 10 with $\lambda_0 = 1.5\mu m$ free space wavelength, $k_x = 0.38 \times 2\pi/\Lambda$ (negative GH shift of maximum magnitude (a)), or $k_x = 0.29 \times 2\pi/\Lambda$ (positive GH shift of $0.33\mu m$, (b)).

grey box of Figure 9. As we can see, the position of giant negative Goos-Hänchen shift overlaps well with the guided mode of the grating in all cases.

Again we study the part of the dispersion curve that is between the light lines of the free space and the substrate (dashed rectangle in Figure 12b) where the incidence from the substrate can be totally reflected. Similar observation to that of the s polarization is made: Goos-Hänchen shift exhibits a large negative value when the guided mode is excited. The maximum of the Goos-Hänchen shift is, for this design case, even larger than that of the s polarization: a negative shift as large as thousands of μm is observed.

A total internal reflection is usually required when discussing the Goos-Hänchen shift. This limits the incidence to come from the substrate side at an angle larger than the critical angle, and it is the part of the dispersion curve between the light lines of the substrate and the free space that is used. Notice that the first band of the grating mode is a positive propagating mode and is below the light line of the substrate. Modes in this band cannot be excited by an incidence from the substrate to achieve a positive Goos-Hänchen shift, unless the whole structure is placed on a prism of higher refractive index, and frustrated total internal reflection (FTIR) is used to excite the modes. The next positive propagating band is the one above the second band gap (see Figure 9), and the part of this band in between the two light lines (not shown in Figure 9) can in principle be used to achieve giant positive Goos-Hänchen shift. However, this usually happen at relatively high frequency, and care must be taken in designing the grating so that the first and higher order diffractions are still evanescent modes at this frequency.

When the incidence comes from the free space side, the grating considered in Figure 10 and Figure 11 give a reflectance that in general is less than 1. To achieve unity reflectance for a broad incidence angle, we can place the grating on top of a perfect electric conductor (PEC) substrate. The PEC surface is responsible for the total reflection while the dielectric grating can help provide a giant Goos-Hänchen shift. It is true that metal has loss issues at optical frequency range. However, a Distributed Bragg Reflector will provide total reflection with negligible loss which functions as a PEC. The principle is similar, that is, giant Goos-Hänchen shift exhibits when a guided mode is excited. Of course, the exact position of the guided mode

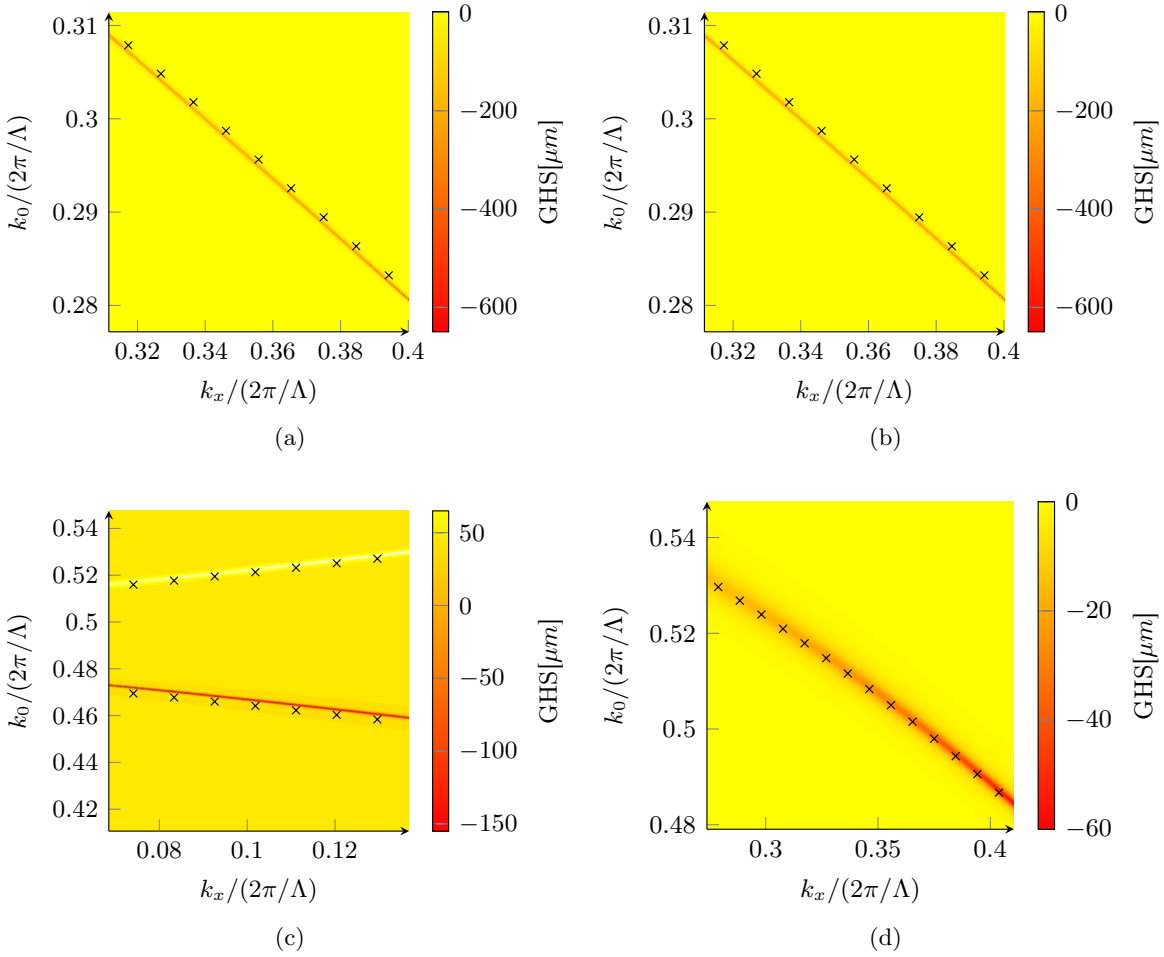

Figure 12: Results for the grey boxes of Figure 9 are given in (a) for s polarization and in (b) for p polarization. (c) corresponds to the same design parameters, excepts that the substrate is a perfect electrical conductor; (d) corresponds to p polarization, same design parameters except that the grating as half the original thickness. The crosses are the eigenmodes of the corresponding gratings.

resonance is different from that of Figure 9. Using an incidence from the air can be more convenient in many situations. Furthermore, since total reflection occurs as promised for any k_x value, incidence close to the surface normal ($k_x \sim 0$) can be used (the case of Figure 12c), so that the guided modes in the positive propagating band at relatively high frequency can be excited without worrying about bringing higher order diffraction modes into propagation: Positive Goos-Hänchen shift can then be realized. We show the simulation results for a dielectric grating on a gold substrate in Figure 12c (s polarization) and Figure 12d (p polarization). For the sake of simplicity, here the PEC is modeled as $\epsilon = -\infty$ with no ohmic loss. Besides the fact that giant negative Goos-Hänchen shift is again observed at the guided mode resonance, several features deserve specific mention. First of all, giant negative Goos-Hänchen shift can be observed for incidence with s polarization. This is contrary to the bare plasmonic substrate case where negative Goos-Hänchen shift caused by surface plasmon only happens for the p polarization, while for s polarization, positive Goos-Hänchen shift is observed. This is another proof that the grating decoration on top of the PEC surface plays a crucial role in achieving the Goos-Hänchen shift. Second, giant Goos-Hänchen shift of positive value is indeed observed at the third eigenmode band, a positive propagating mode above the second band gap. This is shown in Figure 12c (the first band, which is a positive mode band below the light line, is not shown in this plot). As discussed before, the p polarization incidence on metal could excite surface plasmonic resonance and exhibits giant Goos-Hänchen shift, however, with poor reflection rate. Figure 12d shows that p polarization can achieve total reflection and giant Goos-Hänchen shift for free space incidence.

3.3 Conclusion

In conclusion, we have used the guided mode resonance on dielectric gratings to realize giant Goos-Hänchen shift. The giant Goos-Hänchen shift is caused by the coupling of the incidence to the guided mode of the grating which are leaky on the incidence side. The large power flow carried by the guided mode is responsible for the giant Goos-Hänchen shift. By exciting either a positive or a negative propagating mode, positive or negative Goos-Hänchen shift is realized. Since the entire design is based on dielectric structure, ohmic loss can ideally be completely avoided and a unity reflectance can be realized. This is advantageous compared to many of the plasmonic material based approaches. We believe the design has great potential in sensor applications (45; 46). Notice that a large Goos-Hänchen shift happening in a finite reflection phase range ($\sim 2\pi$) usually means a sharp resonance with the incidence angle (Figure 10a), the frequency (Figure 10b), the dielectric constant of the ambient environment, and other parameters. Such sharp resonances can be used for sensing with high sensitivity. The design also has wide application in optical bistability, slow light control, and waveguide dispersion engineering as will be shown in following chapters.

CHAPTER 4

BISTABLE GOOS-HÄNCHEN SHIFT AND PHASE SHIFT BASED ON THE GUIDED MODE RESONANCE

This chapter presents the assessment of guided mode resonance to perform optical bistable functionality. Optical bistability is one of the phenomena exhibited by Kerr-type resonators (47). It is a promising candidate for optical switches and memory applications. In this chapter, we made use of the high quality factor resonant grating cavity to perform bistable Goos-Hänchen shift.

4.1 Optical bistability at a glance

Among research on all-optical interaction, optical bistability phenomena generated interests for research studies with performance of one input state, two possible stable output states. The two different outputs are determined not only by the intensity of the input, but also by the ascending and descending derivatives of the input signal. Optical bistability is a promising feature to be applied to the optical switching and memory systems, specifically in high speed all-optical information processing (48). It was first discovered by Gibbs in 1975 (49), since then numerous nonlinear materials and optical resonant structures have been studied and demonstrated to exhibit the bistate features. In general, there are two types of systems that produce optical bistability: hybrid optical bistable system with electronic feedback circuit involved or intrinsic optical bistable system with light involved only. This chapter focuses on intrinsic op-

tical bistable system. Since for all-optical circuits, speed is one of the most important figures of merit. The optical feedback mechanism is preferable due to a shorter delay compared to electronic circuits.

Intrinsic optical bistable systems must have a resonant feature and normally takes advantage of the nonlinearity of Kerr type material, whose refractive index depends on the optical intensity. Since light intensity influences the refractive index as well as the phase of the electromagnetic field, the resonance frequency ω_{res} of the structure experiences perturbation. In other words, this perturbation due to the resonance influences the amplitude of the electromagnetic field inside the structure hence the intensity. Therefore, a feedback loop is intrinsically built in so that a steady states can be reached eventually.

Regarding optical resonators, several geometries can be good candidates. The most common device would be the Fabry-Pérot cavity which exhibits Airy resonance (50). Photonic crystals possess the potential due to compact size and reduced power (51). Grating couplers that can excite guided mode resonance with easy multiplex/demultiplex at input and output ports are also studied (52). Besides the self-feedback schemes of bistability, systems that use one input signal to control another are also presented. Optical switching was realized in cross-waveguide geometry with one controlling signal and one input signal (53), which can be good candidates for optical transistor. Similar concepts were used in a Kerr type ring resonator, for which one input signal were to control the refractive index of the ring resonator (54). There still exists a great challenge to implement the system mentioned above for all-optical applications. These systems are either too bulky, or require great laser intensity to exceed the threshold. The

reason for the limitations is due to the fact that most materials having very small nonlinear Kerr effects (49; 55).

To make these systems compatible for integrated optics, it is necessary to reduce their threshold intensity. Subwavelength grating and photonic crystals were found to display such advantage. Guided mode resonance can be launched inside the grating with a high quality factor and field confinement (56; 57). A high quality factor provides great field enhancement inside the stricture with respective to the incidence, high field confinement will allow the effective aperture to be very small, for example $(\lambda/5)^2$ in Ref. (58). These features tremendously reduce the threshold power and size of the system, which makes the applications possible.

Most studies are currently focused on the bi-state of the transmissivity which gives a direct signal via optical detectors. Recently, a new bistable phenomenon regarding the Goos-Hänchen shift along the interface has been discovered and demonstrated (59; 60; 61). and could lead to new approaches for delivering information and implementing the applications. As previous chapters mentioned, negative and positive Goos-Hänchen shift could be achieved, which allows more freedom in designing specific components (62) and also lead to various of applications in sensors (45) and slow light devices (63). In this chapter, we are going to introduce the realization of giant bistable Goos-Hänchen shift based on the high quality factor guided mode resonance. We first explain the mechanics of the optical bistability. Then, we describe in detail our device. Finally, we will discuss the potential and future improvement of our device.

4.2 Mechanics of Optical Bistability

The physics behind different bistable systems is similar. Among them, the Fabry-Pérot etalon would be the simplest system to demonstrate the mechanics of optical bistability (64). We use the Fabry-Pérot etalon as an example to explain the details of a bistable system (12; 64). Consider a Fabry-Pérot etalon, a dielectric plate of refractive index n' with that of ambient medium as n, and assume a monochromatic beam is incident upon the plate at incidence angle θ, which is shown in Figure 13. The light is incident on the surface of the plate and divided into a reflected and a transmitted beam. The transmitted beam will again be divided into reflected and transmitted plane waves when the light arrives on the other surface. The process continues infinite times as indicated in the figure. Suppose the amplitude of the electric field of the incident wave is E_0. The polarization is linear and of either 's' or 'p' type. For each reflected or transmitted wave, the phase difference from the preceding one would be twice the amount corresponding to the traversal of the plate. i.e.

$$\Phi_0 = \frac{4\pi}{\lambda_0} n' h \cos\theta \tag{4.1}$$

where h is the thickness of the plate and λ_0 is the wavelength in vacuum. Let r be the reflection coefficient and t the transmission coefficient from the surrounding environment n to the plate n', while r' and t' be the coefficient for plate to the surroundings, respectively. The coefficients

here stand for the ratio between amplitudes of electrical fields. Recalling Fresnel's formula given by Equation 1.1, we would obtain the relation of

$$\begin{aligned} tt' &= T \\ r &= -r' \\ r^2 &= r'^2 = R \end{aligned} \tag{4.2}$$

where R and T are the reflectivity and transmissivity of the plate surface with energy conservation relation

$$R + T = 1 \tag{4.3}$$

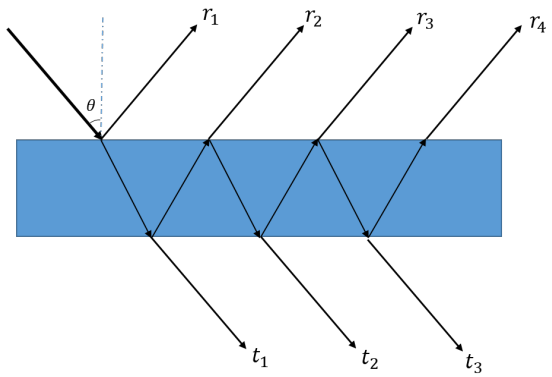

Figure 13: Schematics of Fabry Pérot etalon

The complex amplitudes of the waves reflected each time from the plate's upper surface are then

$$rE_0, \quad tt'r'E_0e^{j\phi}, \quad tt'r^3E_0e^{2j\phi}, \quad ... \quad tt'r'^{2(p-1)}\phi, ... \tag{4.4}$$

Adding the complex amplitudes of the infinite reflected waves yields the total reflected field E_r of the plate:

$$\begin{aligned} E^r &= r + tt'r'e^{j\phi}(1 + r'^2e^{j\phi} + ... + r'^{2(p-2)}e^{j(p-2)\phi}) \\ &= -\frac{r'\{1 - (r'^2 + tt')e^{j\phi}\}}{1 - r'^2e^{j\phi}}E_0 \quad (p \to \infty) \end{aligned} \tag{4.5}$$

Using Equation 4.2 the previous relation is transformed into

$$E_r = \frac{(1 - e^{j\phi})\sqrt{R}}{1 - Re^{j\phi}}E_0 \tag{4.6}$$

and the associated intensity is related to I_{in} according to

$$I_r = \frac{(2 - 2\cos\phi)R}{1 + R^2 - 2R\cos\phi}I_{in} = \frac{4R\sin^2\frac{\phi}{2}}{(1 - R)^2 + 4R\sin^2\frac{\phi}{2}}I_{in} \tag{4.7}$$

where $I_r = \frac{1}{2}c\epsilon_0E_rE_r^*$.

Similarly, from energy conservation considerations the transmitted wave is

$$I_t = \frac{T^2}{(1 - R)^2 + 4R\sin^2\frac{\phi}{2}}I_{in} \tag{4.8}$$

Defining a parameter $\mathcal{F}$ called *finesse* satisfying

$$\mathcal{F} = \frac{4R}{(1-R)^2} \tag{4.9}$$

Equation 4.8 is written as:

$$I_t = \frac{1}{1 + \mathcal{F}\sin^2\frac{\phi}{2}} I_{in} \tag{4.10}$$

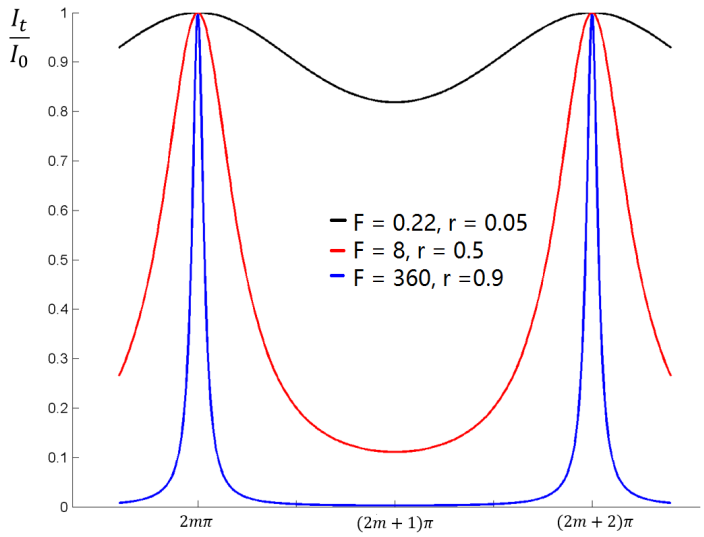

Figure 14: Transmissivity $\mathcal{T} = I_t/I_{in}$ as the function of phase difference ϕ. Multiple beam fringes of equal inclination in transmitted light.

The finesse of Fabry-Pérot etalon is parameter proportional to the quality factor. The total transmissivity $\mathcal{T} = I_t/I_{in}$ as a function of the round trip phase difference ϕ inside the plate is

shown in Figure 14 for various values of the finesses. If the surface reflectivity R is increased, the intensity of the minimal of the transmission decreases, and the transmission peak becomes narrower until R approaches unity. The dielectric plate becomes transparent and the light beam is totally transmitted when the phase difference $\phi = 2m\pi$, which is the resonance condition of the Fabry-Pérot etalon.

As discussed above, the transmissivity of the Fabry-Pérot is determined by the round trip phase difference and the finesse. The transmission will always be unity while at resonance, where the round trip phase delay becomes an integer multiple of 2π. According to Figure 14, the transmission coefficient strongly depends on the phase difference, especially when the finesse has a large value. To realize optical bistablity, nonlinearity must be included into to the system. Consider a plate is made of Kerr type material, which has the property that its refractive index can be changed by the local power of the light according to

$$n = n_L + n_2 I \tag{4.11}$$

where n_L is the linear refractive index of the material while the intensity is zero. n_2 is the nonlinear Kerr coefficient with unit of cm^2/W, I is the local field intensity. For Kerr material, the round trip phase difference ϕ will be denoted as Φ^{NL} (NL: Nonlinear). The transmission coefficient $\mathcal{T}$ is written as

$$\mathcal{T} = \frac{1}{1 + \mathcal{F} \sin^2 \Phi^{NL}} \tag{4.12}$$

where

$$\Phi^{NL} = \Phi_0 + K\mathcal{T}I_{in} \tag{4.13}$$

Φ_0 is given by Equation 4.1 and K is constant proportional to the thickness of the etalon the Kerr coefficient, n_2.

Equation 4.13 provides the nonlinear phase shift resulted from the intrinsic refractive index variation associated with the optical Kerr effect. It indicates a linear relation with the transmissivity and the phase shift Φ^{NL} and its slope is inversely proportional to the input intensity I_{in}. Thus, we can interpret the total transmissivity $\mathcal{T}$ as

$$\mathcal{T} = \frac{\Phi^{NL} - \Phi_0}{KI_{in}} \tag{4.14}$$

The nonlinear system reaches steady states only when Equation 4.12 and Equation 4.14 are satisfied simultaneously. Referring to Figure 15, we show the procedure for the realization of two stable states with one input state. As the intensity increases from zero, the intersection of Equation 4.12 and Equation 4.14 is presented by points 1, 2, 3, 4, 4′, 5, sequentially. Notice that in some situation two or more solutions exist, however, the correct solution falls in the first achieved stable state. A discontinuous transition occurs from point 4 to point 4′, for which point 4 is the point of tangency of the transmissivity curve. In fact, the transmissivity suddenly increases resulting into a higher level output intensity. The input intensity at point 4 is defined as the threshold input I_{th}. When the input intensity I_{in} decreases, the output intensity will form a hysteresis loop not tracing the previous path but following the route of 5, 4′, 3‴, 2′, 2,

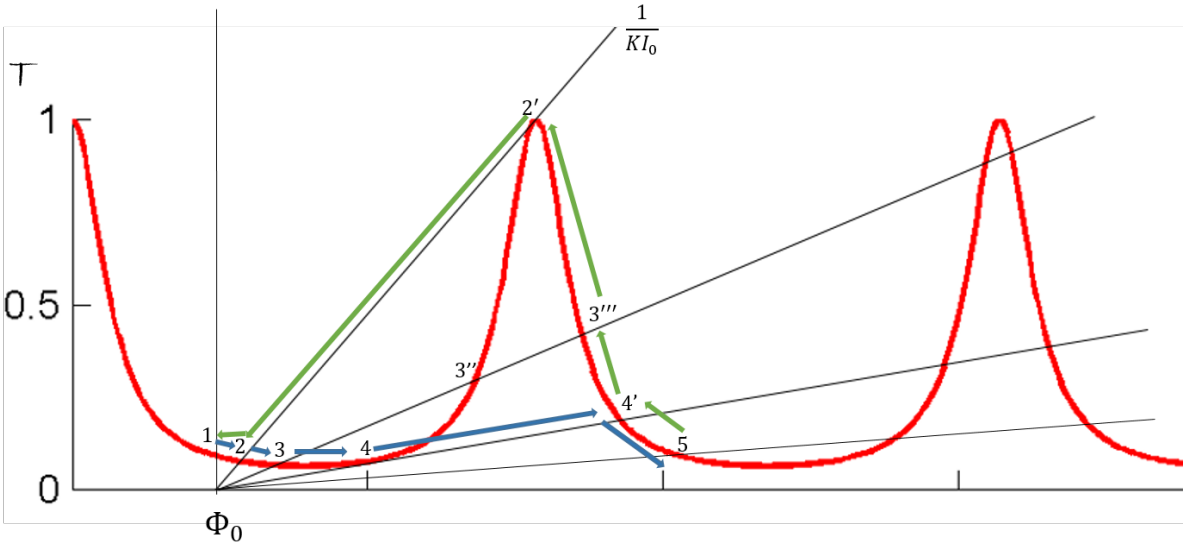

Figure 15: Transmission response analysis for a nonlinear Fabry-Pérot etalon

1. Again, a sudden decay of the transmissivity occurs from point $2'$ to 2 leading to a drastic reduction of the output signal.

The output intensity behavior versus the input is plotted in Figure 16. We can observe that once the input intensity exceed the threshold I_{th}, a hysteresis loop for the output intensity is formed. Within the window of the hysteresis loop, one input state leads to two output states. The output states would not only depend on the magnitude, but also the derivative of the input intensity to time.

4.3 Bistable Goos-Hänchen and phase shift

We present a 1D binary grating made of Kerr type Si material that covers a SiO_2 substrate. Under the condition of total internal reflection, the beam experiences a sharp reflection phase

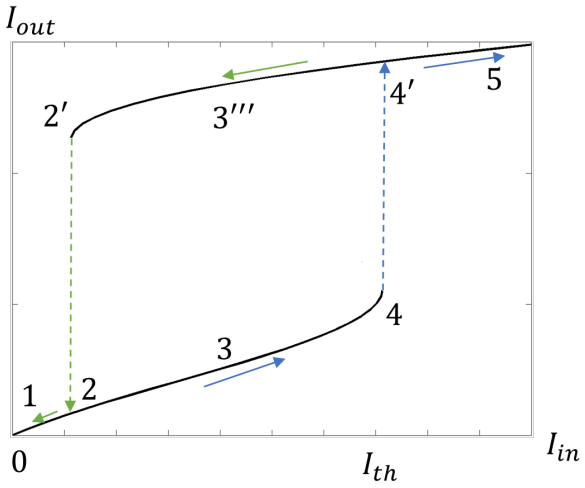

Figure 16: Bistable output intensity towards the input. A general hysteresis loop of bistability is formed

shift and thus generate a large negative Goos-Hänchen shift(62). This phase shift is brought about by the guided mode resonance inside the grating.

The Kerr coefficient of Si is $n_2 = 3 \times 10^{-14} \mathrm{cm}^2/\mathrm{W}$ which is 100 times larger than that of the SiO_2 substrate. Hence, the nonlinearity essentially only applies to the material of the grating while negligible on the ambient environment (the substrate and free space). Since the Kerr coefficient for natural materials is generally small, a high quality factor is essential for operation of a bistable system. The subwavelength grating can achieve a very high quality factor with a level of 10^5 as reported in (65) and theoretically higher. This is particularly advantageous for reducing the threshold intensity I_{th} of the source laser. Moreover, the reflection phase change depends on the guided mode resonance rather than the Fabry-Pérot cavity mode. This leads to a compact size which is important to build integrated chip devices. Since our device has

nano-scale and the transient time of the Kerr effect is small, the bistability result is obtained via a stationary numerical study.

4.4 Bistable phase shift and Goos-Hänchen shift with 1D Kerr grating

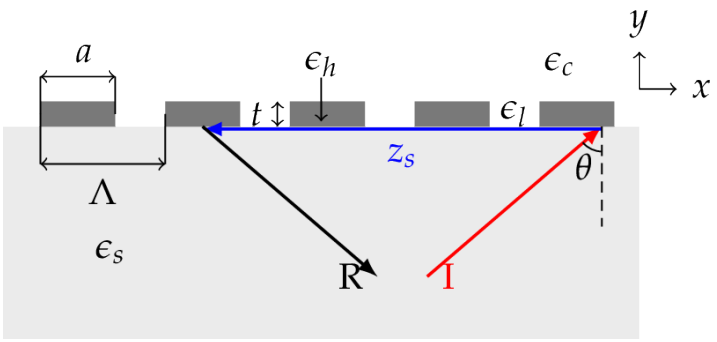

Figure 17: Schematic of a dielectric gating and the GH shift under a TIR. a is the length of the high refractive index dielectric with a period, Λ is the period, the filling factor $F = a/\Lambda$. "I" and "R" refer to the incident and reflected beams respectively. z_s is the negative GH shift. In this experiment, the filling factor $F = 0.99$, period $\Lambda = 373$nm, grating thickness $t = 239$nm, refractive index of the grating $n_g = 3.48205$ while of the substrate $n_s = 1.44462$, the polarization is s with E field perpendicular to the grating groove.

Figure 17 shows a 1D binary grating structure which was described in detail in Chapter 3. The excitation coming from the SiO_2 substrate has an incidence angle above the critical angle thus experiencing total internal reflection, which differs from the normal incidence in (66). As stated in Chapter 3, giant positive and negative Goos-Hänchen shifts were achieved due to the guided mode resonance. The excitation of guided mode resonance is mediated by the reciprocal lattice vector $K = 2\pi/\lambda$ of the grating as for a conventional grating coupler according

to Equation 2.2. The reflection phase from the grating is numerically calculated using the Rigorous Coupled Wave Analysis (37).

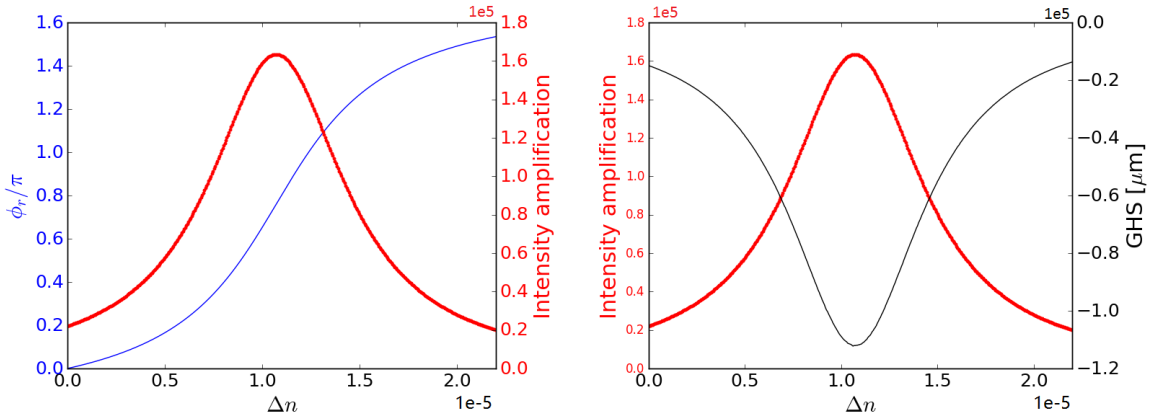

Figure 18: The amplification of the incident intensity inside the grating, reflection phase and Goos-Hänchen shift varying with perturbation refractive index Δn. (a): The intensity amplification and reflection phase. (b) The intensity amplification and Goos-Hänchen shift.

The incident beam strikes the grating from the SiO_2 substrate with a free space wavelength of $\lambda_0 = 1.5\mu$m and the incident angle of $\theta = 39.34°$. The local field intensity inside the grating changes dramatically with small perturbation of the refractive index Δn in a high quality factor system. The parameters of the grating are designed to achieve a theoretical quality factor of 4.23×10^4. For the grating structure to provide giant negative Goos-Hänchen shift, the reflection phase and hence the Goos-Hänchen shift will vary as well as shown in Figure 18.

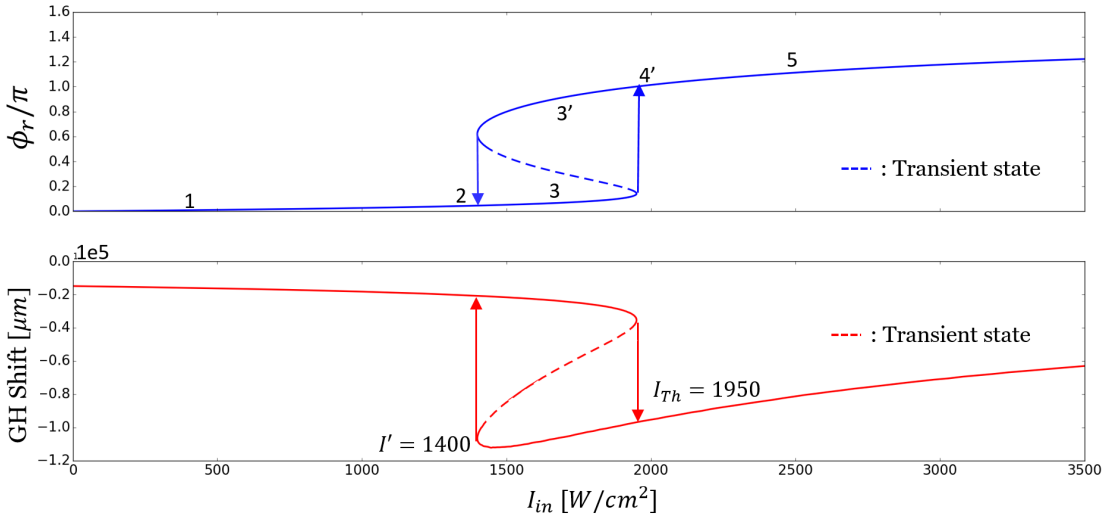

Figure 19: Optical phase (top figure) and Goos-Hänchen shift (bottom figure) bistability with the variation of the input field intensity. The threshold input intensity $I_{th} = 1950\text{W/cm}^2$ and the backward threshold intensity $I'_{th} = 1400\text{W/cm}^2$ for both phase and GH shift bistability. The solid lines show the steady state of the system while the dashed line represents the transient states. The arrows show the directions of switching as the input intensity increases or decreases.

Note that in Figure 18, the local field is represented by the field amplification, Amp. More interestingly, the reflection phase of the incident beam experiences an almost 2π shift within extremely small change of grating's refractive index as shown in Figure 18a. It has a promising potential for applications in optical modulation, exhibiting a phase modulation range over π. Also, the negative Goos-Hänchen shift appears to display a one to one correspondence with the local intensity enhancement in Figure 18b. We can obtain the phase and Goos-Hänchen shift response to the input field intensity subject to $I_{in} = Amp \times I_{loc}$ and $\Delta n = n_2 I_{loc}$, where I_{loc}

is the local field intensity. We discovered that the Kerr material grating leads to a bistable reflection phase and Goos-Hänchen shift which are shown in Figure 19. The reflection phase increases by 0.9π for the forward switch (state 4 to $4'$) while it decreases 0.6π for the backward process (state $2'$ to 2). Simultaneously, the amplitude of negative Goos-Hänchen shift switches at $6.3 \times 10^4 \mu$m or $4200\lambda_0$ for the forward process while it switches $8.8 \times 10^4 \mu$m or $5867\lambda_0$ for the backward one. The forward threshold field intensity is $I_{th} = 1950\text{W/cm}^2$ while the backward threshold field intensity is $I' = 1400\text{W/cm}^2$. The intensity window for the bistable states is $\Delta I = 550\text{W/cm}^2$. The window size is determined by both the quality factor and the initial state, which are provided by Figure 13. The threshold field intensity is comparable with $I_{th} = 1400\text{W/cm}^2$ in (61). However, the Goos-Hänchen shift change obtained is more than 200 times, which provides a more distinct switching state. Among the three structural parameter of the grating, the period Λ determines the resonance frequency, while the other two, the filling factor F and grating thickness t, influence the quality factor. The analysis of the quality factor is shown in Figure 20 and it indicates that a larger filling factor F results in a greater quality factor. However, the thickness of the grating should be also considered because maximum quality factor are achieved among the grating thickness from 240nm to 260nm. In Figure 20b, the incident angle decreases while increasing either the filling factor or the grating thickness. The bottom left corner of Figure 20b indicates that while filling factors and grating thickness are both low, the resonance incident angle approaches the grazing angle. On the contrary, the top right corner shows that the incident angle approaches the critical angle $\arcsin(1/n_{sub}) = 43.8^\circ$ when both filling factor and grating thickness are high. This behavior could result in reducing

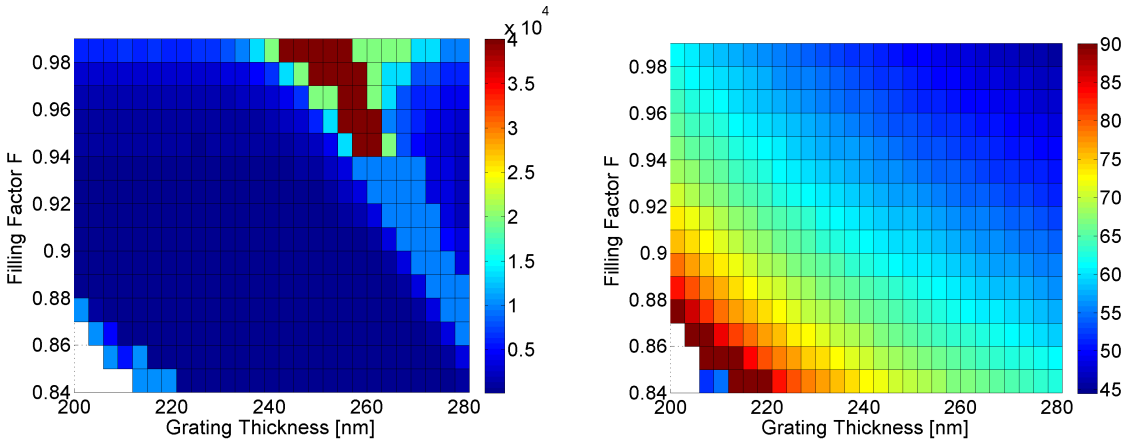

(a) (b)

Figure 20: The quality factor and corresponding resonant incident angle for the grating design. The y axis is the filling factor while the x axis is the thickness of the grating. The free space resonant wavelength is $1500nm$ while the period $\Lambda = 373nm$. (a): The quality factor. (b): The incident angle for resonance.

the quality factor as shown in Figure 20 since the critical angle is the boundary of the radiative or non-radiative regions in the dispersion relation.

4.5 Conclusion

In this chapter, we introduced another approach to achieve optical bistability by implementing the Goos-Hänchen shift rather than the general bistable transmission scenario. By taking advantage of the high quality factor feature of the guided mode resonance and of the low loss of dielectric material, it is feasible to design a grating achieving very high distinct bistable state with relatively low laser intensity input. We demonstrated an example of giant bistable Goos-Hänchen shift and phase shift with extremely large quality factor. The Goos-Hänchen shift bistability could be applied to the positional sensor while the later could be more important

for modulation and switches. The feasibility of designing the quality factor of the grating is also demonstrated. The grating parameters can be selected to fit the fabrication limits, input laser power and frequencies. The input threshold power can be further reduced by selecting artificial Kerr material which are hundreds times higher than natural material. The bistable Goos-Hánchen shift and phase shift are very promising features to be further investigated and applied to optical circuits.

CHAPTER 5

BROADBAND LIGHT SIGNAL TRAPPING BASED ON NEGATIVE GOOS-HÄNCHEN SHIFT

***Disclaimer**: This chapter is reproduced from published paper — Rui Yang, Wenkan Zhu, Jingjing Li, "Realization of "trapped rainbow" in 1D slab waveguide with Surface Dispersion Engineering" Opt. Express 23, 6326-6335 (2015). The author of this thesis was the main contributor to the publication.*

This chapter presents a design of a one-dimensional dielectric waveguide that can trap a broadband light signal with different frequency components stored at different positions, effectively forming a "trapped rainbow". The spectrum of the rainbow covers the entire visible range. To do this, we first show that the dispersion of a SiO_2 waveguide with a Si grating placed on top can be engineered through the design parameter of the grating. Specifically, guided modes with zero group velocity (frozen modes) can be realized. Negative Goos-Hänchen shift along the surface of the grating is responsible for such a dispersion control. The frequency of the frozen mode is tuned by changing the lateral feature parameters (period and filling factor) of the grating. By tuning the grating feature point by point along the waveguide, a light pulse can be trapped with different frequency components frozen at different positions, so that a "rainbow" is formed. The device is expected to have extremely low ohmic loss because only dielectric materials are used. A planar geometry also promises significantly reduced fabrication difficulty.

5.1 Review of Light Trapping Schemes

To use photons as information carriers is currently under intense study because of the almost unlimited bandwidth and the high energy efficiency. Many devices in an optical network depend on the capability to control the dispersion property of a waveguide. One example is the slow light for which the group velocity of light is much smaller than that in the free space. Applications of slow light devices include optical buffers, nonlinear optics, and optical signal processing. Whereas the slow light is usually realized on Bose-Einstein condensate (67), building solid-state slow light devices is of great practical importance. The former is based on electromagnetically induced transparency (EIT) and usually demands bulky, ultra-low temperature apparatus, while the latter is of much lighter weight and is applicable for on-chip integration. Photonic crystals are used almost exclusively for on-chip slow light devices. Usually, the part of the dispersion curve around the edge of the reduced Brillouin zone is used. This part of the dispersion curve are flattened because of the coupling between the forward and backward propagating modes, and exhibits a very small group velocity (68; 69; 70; 71). In 2007, a new idea to realize slow light was proposed in theory by Tsakmakidis, et. al., making use of the anomalous property of metamaterials (72). In their proposal, the negative Goos-Hänchen shift on a interface between a metamaterial and a regular dielectric is used. It was shown that, for a waveguide made of a metamaterial, when the Goos-Hänchen shift on the side walls of the waveguide compensates completely the forward-leap of the ray in a round trip, the guided mode would become, intuitively, "frozen" on the waveguide and no forward power propagation can be observed. This is actually a description of slow light using the ray picture. Further, a scheme of

trapping optical signals of a broad frequency band is proposed: since the operating frequency to freeze the light is related to the waveguide thickness, a waveguide segment of tapered thickness should be able to trap light of a continuous spectrum at different positions along the waveguide, forming a "trapped rainbow".

This idea has since attracted many researchers and different designs have been attempted. However, the experimental realization of the original idea of "trapped rainbow" faces great challenge. In the original design, the metamaterial was treated as a homogeneous medium similar to a regular dielectric, while in reality such an artificial material is always composed of discrete inclusions with strong temporal and spatial dispersion. Up to now, the best optical metamaterial uses inclusions of $\sim \lambda_0/3$ in size, where λ_0 is the free space wavelength at the operating frequency. When used to build a waveguide which itself might only be a few wavelengths in width, the modeling of the waveguide as a homogeneous one is problematic. The optical metamaterial usually operates at a frequency up to the near infrared. Little progress has been made for metamaterials working in the visible band with reasonably good properties. Also, metamaterials are inevitably dispersive, and there have been no report on metamaterials with negative ϵ and/or μ that cover the entire visible domain. Further, the ohmic loss related with metamaterial is a formidable factor. In the optical frequency domain, plasmonic materials (gold or silver) are used almost exclusively to build metamaterials. Their ohmic loss is far from tolerable for the application of "trapped rainbow", and might erase any feature related to the broadband rainbow trapping. There have been a few reports on the experimental demonstration of the "trapped rainbow" after the theoretical proposal (73; 74; 75). However, none

has actually used the approach proposed in the original paper that was based on the negative Goos-Hänchen shift. Rather, they are realized on the edge of the Brillouin zone of a plasmonic periodic structure. Inevitably, the strong ohmic loss makes the trapping effect very weak.

In this chapter, we numerically demonstrate an approach to realize frozen mode based on the negative Goos-Hänchen shift. The proposed approach uses only dielectric materials, thus could have extremely low ohmic loss. The "trapped rainbow" is then realized by a waveguide with chirped or adiabatically tuned design of the frozen mode waveguide. We believe our approach is the first, complete demonstration for a frozen mode and trapped rainbow that uses the negative Goos-Hänchen shift, the original idea in Ref. (72). In the following, we first review the idea of using negative Goos-Hächen shift to construct a frozen mode, and our recent discovery that negative Goos-Hänchen shift, sometimes of giant magnitude, can be realized on the surface of a dielectric covered by a grating. We then demonstrate rigorously that a "frozen mode" where the Goos-Hänchen shift fully compensates the forward leap of the ray in a round trip inside a slab waveguide indeed corresponds to zero group velocity of the guided mode, and show numerical results of such a frozen mode. Based on this waveguide that supports frozen mode, we then show our designs of the "trapped rainbow" concept, for which a broadband pulse is stopped with different frequency components trapped on different positions along the device.

5.2 Theory of Negative Goos-Hänchen Shift and Frozen Mode

We would like to realize Tsakmakidis's idea (72) to form a frozen mode using a dielectric grating to obtain the Goos-Hänchen shift, as discussed in Chapter 3. We recall that, mathemat-

ically, the Goos-Hänchen shift can be evaluated according to Equation 1.6 which is rewritten here for convenience,

$$z_s = -\frac{\partial \phi}{\partial k_x} \tag{5.1}$$

where ϕ is the phase of the reflection coefficient of the plane wave component with a lateral wavenumber of k_x. The Goos-Hänchen shift is usually positive for the reflection from an interface between two regular dielectrics, while negative for interfaces between regular dielectrics and plasmonic material or metamaterial.

The negative Goos-Hänchen shift has attracted considerable research interests, one of which is to control the direction of energy flow in a dielectric slab waveguide with respect to the wave vector of the guided mode, as discussed in the same paper that proposed the trapped rainbow (72). Whereas the original discussion was from a rather intuitive approach, here we would like to give a rigorous mathematical description. Consider a slab waveguide made of a dielectric of refractive index n and thickness h. A guided mode can be described as a plane wave totally internally reflected back and forth on the two interfaces that satisfy the following relationship:

$$2nhk_0 \cos\theta + \phi_1(\theta, k_0) + \phi_2(\theta, k_0) = 2m\pi \tag{5.2}$$

where k_0 is the free space wavenumber, θ is the angle of incidence, $\phi_j(\theta, k_0)$, $j = 1, 2$ is the phase loss (the phase of the reflection coefficient) on the two side walls, respectively, with m an

integer. When written in terms of k_x, the wavenumber parallel to the waveguide wall, we find that

$$2h\sqrt{n^2k_0^2 - k_x^2} + \phi_1(k_x, k_0) + \phi_2(k_x, k_0) = 2m\pi \tag{5.3}$$

Taking the total differential of both sides with respect to k_0 and k_x, we get

$$2nh\frac{\Delta k_0}{\sqrt{1 - k_x^2/(nk_0)^2}} - 2h\frac{k_x}{\sqrt{n^2k_0^2 - k_x^2}}\Delta k_x + \sum_{j=1,2}\left(\frac{\partial\phi_j}{\partial k_0}\Delta k_0 + \frac{\partial\phi_j}{\partial k_x}\Delta k_x\right) = 0 \tag{5.4}$$

which is a relationship a guided mode must satisfy in addition to Equation 5.2. When deriving the former equation, we assume that n does not change with frequency, which is a reasonable assumption for dielectric waveguides. Divide both sides by Δk_x and take the limit of $\Delta k_x \to 0$, we get

$$\left(\frac{2nh}{\sqrt{1 - k_x^2/(nk_0)^2}} + \sum_{j=1,2}\frac{\partial\phi_j}{\partial k_0}\right)\frac{\partial k_0}{\partial k_x} = 2h\frac{k_x}{\sqrt{n^2k_0^2 - k_x^2}} + \sum_{j=1,2} -\frac{\partial\phi_j}{\partial k_x} \tag{5.5}$$

Notice that $\partial\phi_i/\partial k_0$ is always positive. This is because $\partial\phi_i/\partial k_0$ is the delay of the center of the Gaussian pulse at the reflection of the interface. For a lossless reflection (which is the case here), this delay must be positive for a causal system. This means the sign of the right hand side completely determines the sign of $\partial k_0/\partial k_x$, which is proportional to the group velocity. For the right hand side, the second term is the Goos-Hänchen shift on the two side walls. Also notice that $k_x/\sqrt{n^2k_0^2 - k_x^2} = k_x/k_y$. Thus, if we let $z_w = hk_x/\sqrt{n^2k_0^2 - k_x^2}$, z_w is actually the forward displacement of the ray when propagating from one side wall to the other (see Figure 21a). Combining the contribution of z_s and z_w together, the right hand side of Equation 5.5 gives

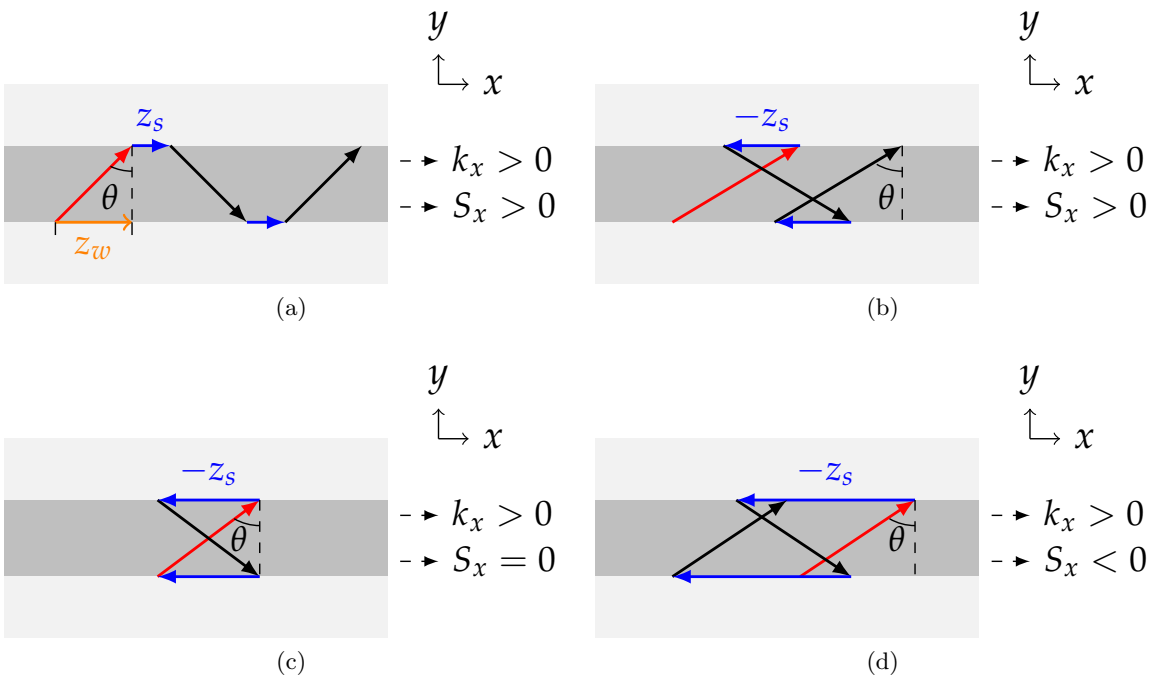

Figure 21: Energy flow and Goos-Hänchen shift in a planar waveguide . The incidence is colored in red, Goos-Hänchen shift z_s in blue, while the forward displacement z_w in orange. The rays travels inside the waveguide are in black.

the total x direction displacement of a ray in a round trip, as we see in Figure 21. When the waveguide and the surrounding medium are both made of regular dielectrics, the Goos-Hänchen shift is positive, thus the right hand side is always positive. This means $\partial k_0/\partial k_x > 0$ is always satisfied. Matters become interesting when we have negative Goos-Hänchen shift on one or both of the side walls, especially when it is of large magnitude so that the total displacement is negative (Figure 21d). In this case, the group velocity would be negative, and the energy propagates anti-parallel to k_x. When the Goos-Hänchen shift is just enough to make the right hand side go to zero (the situation described by Figure 21c), we satisfy $\partial k_0/\partial k_x = 0$, and a "frozen mode" of the waveguide is formed. This is a guided mode with finite propagating constant, but zero net power propagation. All these conclusions are consistent with those in Ref (72) but based on rigorous mathematical analysis. We would like to point out that the conclusions only hold when the waveguide material has no temporal or spatial dispersion, i.e. $\partial n/\partial k_0 = 0$ and $\partial n/\partial k_x = 0$, as assumed when deriving Equation 5.4. This is a reasonable assumption for dielectric waveguide, but not for metamaterial waveguides.

5.3 Realization of Frozen Mode Based On Negative Goos-Hänchen Shift Grating

A negative Goos-Hänchen shift is crucial in building a frozen mode. This can be achieved on the surface of plasmonic materials or metamaterials, but is usually accompanied with large ohmic losses. However, it is possible to make negative Goos-Hänchen shift using pure dielectric devices, as we demonstrated in previous chapters and in our publication (62). The system under consideration is shown in Figure 8, where a thin grating made of Si is placed on a substrate of

SiO_2. For certain grating design, the phase of the reflection coefficient for incidence from the SiO_2 side is of very different nature compared to that on the SiO_2/Air interface, as we see in Figure 22 in which s polarized incidence is studied, i.e. E_z is the only electric field component. Whereas the phase decreases with the incident angle for a SiO_2/air interface indicating a positive Goos-Hänchen shift (see black dashed line in Figure 22), on the SiO_2/grating interface, the phase increases, exhibiting a negative Goos-Hänchen shift (see red solid line and black solid line in Figure 22). This is similar to that of a SiO_2/Metamaterial case (see red dashed line in Figure 22). The negative Goos-Hänchen shift is related to the guided mode of the grating. For the second band of the guided mode of the grating, the energy propagates to the opposite direction of the wave vector. The part of the dispersion curve for this band that is between the light lines of the free space and the substrate is leaky on the substrate side, and can couple to the incident beam efficiently. The amount of Goos-Hänchen shift can be controlled by the grating design: depending on the parameters of the grating, we may have a very large (a steep ϕ-k_x curve) or a mediocre (a slow-varying ϕ-k_x curve) Goos-Hänchen shift. In fact, the amount of Goos-Hänchen shift ranges from tens of nanometers up to several millimeters.

With the aid of the negative Goos-Hänchen shift on the grating, we can readily realize the frozen mode discussed in the former section, by placing the grating on the sides of a dielectric waveguide. It turns out that grating on one side is sufficient to realize our goal. One of the designs makes use of a SiO_2 waveguide of 200nm thick and a grating of 40nm in thickness. The schematic of the design is shown in Figure 23.

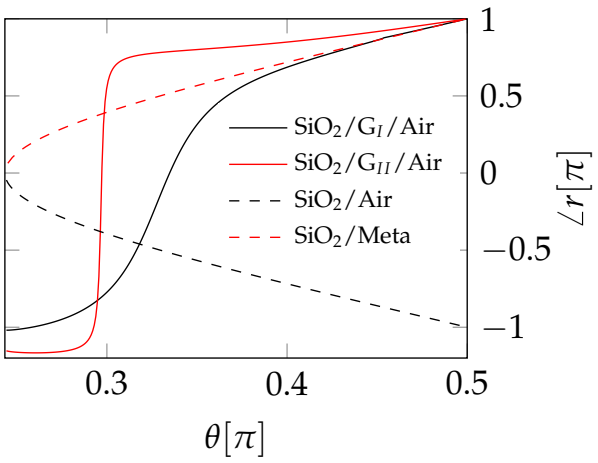

Figure 22: Reflection phase vs incidence angle θ for different interfaces when incidence is from the SiO_2 substrate. Operating free space wavelength is 1.5μm. Grating$_I$ parameters: $\Lambda_I = 0.53\mu$m, $t_I = 0.097\mu$m, $F_I = 0.65$. Grating$_{II}$ parameters:$\Lambda_{II} = 0.43\mu$m, $t_{II} = 0.11\mu$m, $F_{II} = 0.93$.

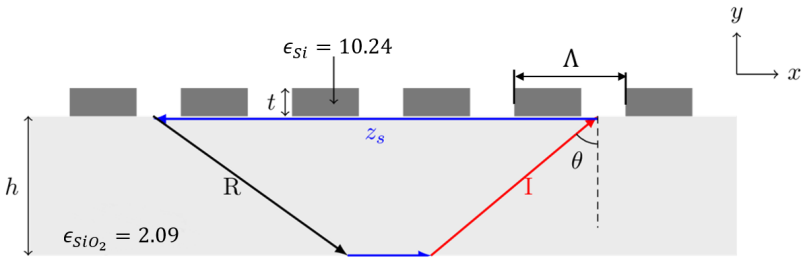

Figure 23: The schematic for a frozen mode design. The circulating rays depict the frozen mode using geometric optics.

In order to calculate the dispersion curve of this grating-decorated waveguide, we first find out the reflection phase $\phi(k_0, k_x)$ on the SiO_2/Grating interface and the SiO_2/Air interface, respectively. These values are then used in Equation 5.2 to obtain the dispersion relation. The results are shown in Figure 24 as red cross. Notice how the dispersion curve bends to form a local extreme, $\partial k_0/\partial k_x$ goes to zero where a frozen mode is formed. Calculation confirms that the right hand side of Equation 5.5 indeed approaches zero at the top of the dispersion curve, which demonstrates the application of Equation 5.5 in finding a frozen mode. The numerical evaluation also shows that the right hand side of Equation 5.5 is positive for the part of the dispersion curve with k_x smaller than that at the top point, and negative when k_x is larger than that at the top. This is consistent with the positive or negative group velocity the dispersion curve shows (see Figure 21). The nature of the negative Goos-Hänchen shift can be used to understand the frozen mode. Recall that the negative Goos-Hänchen shift is usually explained by an energy flow beyond the reflection interface that is opposite to k_x (15). If this power flow compensates completely the forward power flow inside the waveguide, no net power flow is carried by the guided mode, and a zero group velocity is expected.

The evaluation of the dispersion relation using Equation 5.2 assumes that high order spatial harmonics of the field around the grating may be neglected. To verify this assumption, we also evaluated the dispersion relation of the waveguide using full wave analysis. To do this, we use MEEP, an open source numerical electromagnetic package based on the finite-difference, time-domain (FDTD) method (38). The result is shown as circles in the same plot of Figure 24, together with the guided modes of the same Si grating sitting on a SiO_2 substrate of infinite

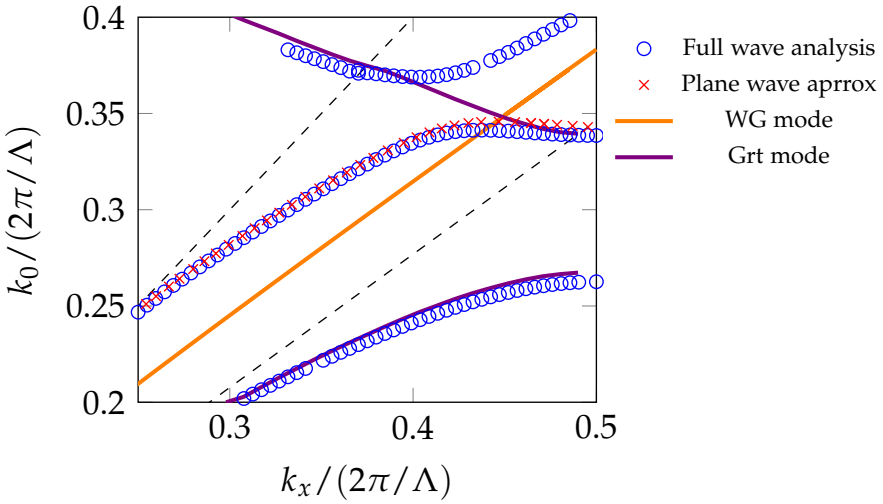

Figure 24: The dispersion property of waveguide with grating parameters: $t = 0.04\mu$m,$\Lambda = 0.16\mu$m, $F = 0.6$, $\epsilon_h = 10.24$, $\epsilon_l = \epsilon_c = 1$; waveguide parameters: $h = 0.2\mu$m, $\epsilon_s = 2.09$. The upper and lower dashed lines are light lines of free space and the waveguide. The blue circles stands for the FDTD result while red cross stands for the plane wave approximation analysis. The solid violet line shows the dispersion of single grating laying on a SiO_2 substrate, while the solid orange line shows the dispersion of bare waveguide.

thickness. We can identify the nature of each part of the dispersion curve by examining the field distribution of the guided modes. For the lowest band below the light line of SiO_2, the electromagnetic field is well confined inside the grating, and the dispersion curve overlaps well with the guided mode of the grating on SiO_2 substrate. These modes are below the light line of SiO_2 and does not couple well with the propagating plane waves in the SiO_2 waveguide, thus can not be predicted by Equation 5.2. Rather, this is the guided mode of the grating itself. The second band is above the light line of SiO_2, thus the plane waves inside the SiO_2 slab waveguide take part in the formation of this band. Notice that the dispersion curve calculated from Equation 5.2 (plotted as red "×") indeed overlaps well with that calculated from full-wave analysis. This means the high order spatial harmonics of the field do not contribute sufficiently in forming the mode, and using Equation 5.2 for mode calculation is a safe approximation. The shape of the lower part of the second band is similar to the dispersion curve of a bare SiO_2 slab waveguide of the same thickness, but shifted in k_x because of the changed reflection phase on the SiO_2/grating wall (see Equation 5.2).

As the frequency increases, the waveguide mode approaches the second band of the grating's guided mode where the two anti-cross each other, causing the opening of a bandgap. Notice that, the second band of the grating mode is also where negative Goos-Hänchen shift is observed (62). The instantaneous field distribution of the frozen mode, i.e. the mode at the top of the lower band, is shown in Figure 25a. It is then obvious for higher frequency frozen mode, which is the bottom of the third band depicted in Figure 24, to show the frozen mode mostly

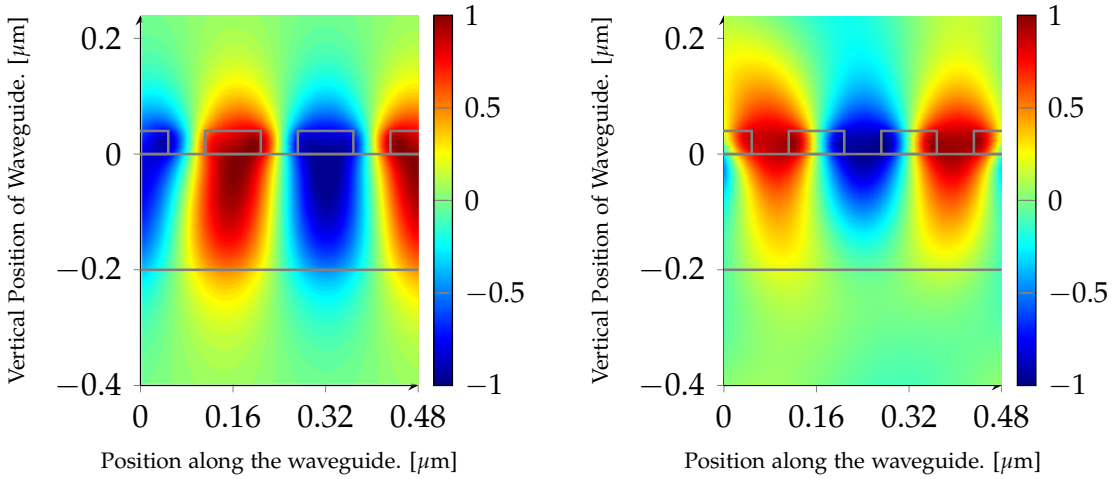

Figure 25: The instantaneous field distribution of the frozen mode in three periods of the waveguide.(a) refers to the frozen mode and top of the second band while (b) refers to the frozen mode of the bottom of the third band.

concentrated in the grating Figure 25b. The Poynting vector evaluated from these simulation results indeed confirm the zero net power flow of these modes.

5.4 Trapped Rainbow Design

One important feature needed for a trapped rainbow is the capability to tune the frequency of the frozen mode. In the original paper about trapped rainbow (72), this is realized by varying the thickness of the waveguide. A tapered waveguide requires gray-scale etching, which is difficult in the conventional micro- and nano- fabrication developed for planar geometry. The grating used in our device can tune the operating frequency without thickness variation: we can change the lateral design parameters (the period Λ and the filling factor F) to modulate

the frequency of the frozen mode while leaving the waveguide thickness untouched. It appears that the frozen mode frequency can be varied most effectively by changing the period. The effect is shown in Figure 26, for the the dispersion curves of two waveguides of the same SiO_2 slab and grating thickness (200 nm and 40 nm, respectively) but different grating periods (blue $\circ$): $Period = 160$ nm; red $\triangle$: $Period = 170$ nm.) The result in this plot is again from MEEP simulation. As we can see, the frequency of the frozen mode (the top of the lower band) is obviously changed. For a period variation of $\sim 6\%$, the frequency is changed by $\sim 4.5\%$.

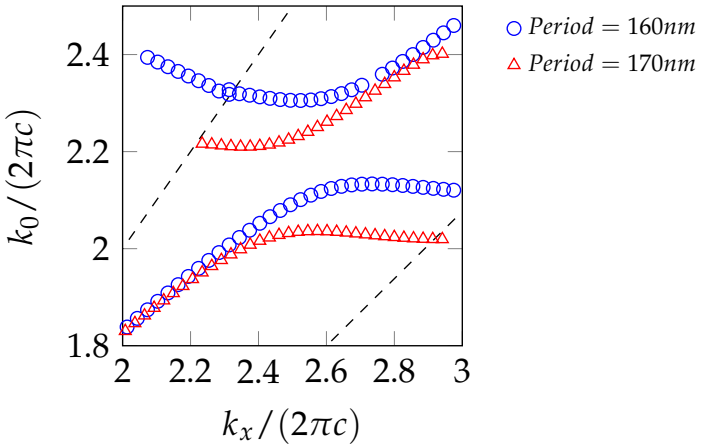

Figure 26: The dispersion of two types of waveguide in the difference of $Period = 0.16\mu$m(Blue circle) and $Period = 0.17\mu$m(Red triangle).

To construct a trapped rainbow requires building a waveguide on which the frozen mode is of different frequency at different position along the device. In our design, this is realized

by placing multiple segments of the waveguide of different grating period one after another. A schematic is shown in the top of Figure 27a. As a demonstration, our first device is composed of 14 waveguide segments, and the grating of each segment consists of 10 identical periods. These gratings have the same thickness of $t = 40$ nm and filling factor $F = 0.6$, but the period varies from 130 nm to 260 nm. The free-space wavelength of the frozen mode that would be supported by waveguides of these different designs range from 395 nm to 704 nm. A broad band pulse is then fed to the device from the left. We arrange the waveguide segments so that the frozen mode frequency decreases from left to the right, with the segments of higher frequency sitting at the upper stream of the optical power flow. This is because, according to Figure 24 and Figure 26, each segment actually supports two modes of zero group velocity, one at the top of the lower band while the other at the bottom of the top band. In our design, we use the lower band of every segment, and the arrangement described above promises that the bottom of the upper band of each segment falls inside the bandgap of its neighboring upper stream segment, thus would not be excited. The structure is again simulated in MEEP. In the simulation, we record the field at different positions along the center of the waveguide after the transient field fades out. A Fourier transform then reveals the spectrum at each position. The observed spectrum intensity at different positions along the whole device is shown in the bottom of Figure 27a. Here the horizontal axis is the lateral position along the device with the origin at the beginning of the first waveguide, while the vertical axis is the signal frequency. The color shows the spectrum intensity. In the simulation, a pulse signal with approximately flat spectrum in the band of interests is used, so that no frequency component has an advantage

in the power intensity. As we walk from left to the right along the device, we can indeed observe 14 discrete steps in the spectrum at positions corresponding to the 14 waveguide segments (the last one is less obvious due to the reflection by the segments ahead of it), going from 760 THz (violet color) to 400 THz (red color). To give an intuitive understanding to the result, we show the color that would be observed at different positions along the device rendered from the spectrum measured at the very position. The algorithm to render a color from a distribution of spectrum intensity is discussed in Ref. (76), and the result is shown in the middle of Figure 27a. The result clearly gives a "rainbow" trapped along the device.

The former demonstration uses a piecewise continuous design. To have a rainbow with adiabatic color change, we turn to a device with tapered design. Rather than physically tapering the thickness of the slab waveguide, we use continuously varying grating period along the whole device in the same range as for the former example, as in we see in the schematic shown on the top of Figure 27b. We expect the result to be a smooth-out version of the trapped rainbow shown in Figure 27a. The result indeed proves our expectation (refer to the middle of Figure 27b). As we see in the bottom of Figure 27b, the peak frequency of the spectrum changes as the observation position changes, and a rainbow of continuously varying color can be observed.

5.5 Method

5.5.1 Rigorous Coupled Wave Analysis

For Figure 22, 25a and part of Figure 24, we used the Rigorous Coupled Wave Analysis (RCWA) based on the algorithm presented by Li (37). When used for the simulation of gratings,

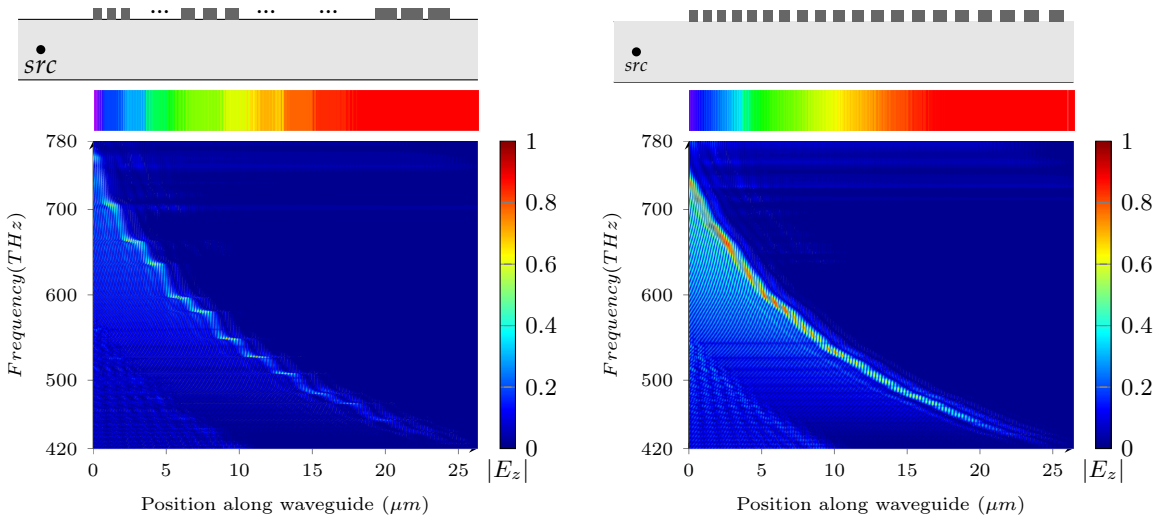

Figure 27: The trapped rainbow field distribution corresponds to the position and frequency. Top: The schematic of the rainbow-trapping device composed of multiple waveguide segments. Bottom: Full wave analysis of the trapped rainbow obtain by FDTD simulation and Fast Fourier Transform. For the waveguide, $t = 0.2\mu$m. (a): For the grating, $F = 0.6$, $t = 0.04\mu$m, period range is designed from $0.13 \rightarrow 0.26\mu$m. The Gaussian pulse enters from the left of the structure in the slab waveguide(not shown in the plot). Both figures demonstrate the field distribution in the frequency domain(vertical axis) and the spatial position(horizontal axis). (a): Rainbow trapping by waveguide of continuously varying parameters. The period varies from 0.130μm to 0.267μm gradually. The other design parameters and the excitation are the same as in (a).

the structure is modeled as a stack of layers periodic in the $x-y$ plane. In each layer, the electromagnetic field is expanded using the eigenmodes of the very layer as the base functions. According to Bloch theorem, the eigenmodes can be written as

$$\mathbf{\Psi}_l(x,y,z) = \psi_l(x,y)\exp\left(ik_{zl}z\right)\exp(ik_x x + ik_y y) \tag{5.6}$$

where $\mathbf{\Psi}$ is either the electric field $\mathbf{E}$ or magnetic field $\mathbf{H}$, and $\psi_l(x,y)$ is a periodic function in $x-y$ plane, l is the order of the eigenmode. k_x and k_y are the lateral wavenumbers that are usually determined by the incidence angle, and k_{zl} is the propagating constant in z direction of the corresponding eigenmode, which is evaluated from the eigenvalue. In RCWA, the eigenmodes of each layer are first solved by expanding the periodic function $\psi_l(x,y)$ into Fourier series. The boundary conditions between neighboring layers are then enforced by equating the lateral components (x and y components) of the electric and magnetic field of the same spatial components in both layers, respectively. Since the geometry of our structure is one-dimensional, we take into account spatial components of orders in $[-25, 25]$ in the x direction (the direction perpendicular to the grating lines), while in the y direction we only take into account the 0^{th} order. Care was taken to verify that this many Fourier orders give good enough precision.

5.5.2 Finite Difference Time Domain Simulation

The FDTD simulation was done on an open source software MEEP (38). For the corresponding results in Figure 24 and Figure 26, we constructed a period of the grating or grating decorated waveguide and used Bloch boundary conditions on the boundaries at $\pm x$ directions.

Perfectly matched layers are used for the $\pm z$ boundaries. A Gaussian pulse is used as the source, and the propagating modes are evaluated from the recorded time series of the electromagnetic field by harmonic inversion (77).

For the results in Figure 27a and Figure 27b, a broadband Gaussian source is used. We record the electromagnetic field only after sufficient running time to allow the transient field to die out. The field is recorded on different positions along the center of the waveguide. A Fast Fourier Transform is carried to give the signal in frequency domain. For the rainbow plots (the middle panels of Figure 27a and Figure 27b), the color at each position was rendered using the evaluated spectrum at the same position, following the method given in Ref. (76). This gives a realistic image of how would the device look like in real life.

5.6 Conclusion

In this chapter we made use of the negative Goos-Hänchen shift on the surface of a dielectric grating to realize a frozen mode, i.e. a guided mode on a waveguide with no net power propagation. Further, by tuning the design parameters of the grating on a waveguide, we can achieve frozen modes with different frequencies sitting at different positions along the waveguide, so that a broad band pulse covering the whole visible spectrum can be caught by the waveguide, with different frequency components stored at different positions. The current design is, to the best of our knowledge, the first demonstration of the "trapped rainbow" proposed in (72) that makes explicit use of the negative Goos-Hänchen shift, the mechanism originally proposed in that paper. At the same time, the use of only dielectric materials promises a much lower ohmic loss. The negative Goos-Hänchen shift is realized on the surface of a grating, which has

a geometry much simpler to be fabricated compared to the usual three dimensional structure of a metamaterial. Tuning the lateral design parameters rather than the thickness further reduces the fabrication difficulty. All these features make the device suitable for practical use in areas such as slow light propagation devices.

It should be pointed out that the "trapped rainbow" serves as a manifesto of the capability of the grating in controlling the dispersion property of a slab waveguide. According to Equation 5.5, the Goos-Hänchen shift, or more generally, the reflection phase ϕ on the surface of the grating, directly determines the behavior of the group velocity. Since the reflection phase is controlled by the design parameters of the grating, Equation 5.5 gives us a straightforward method to synthesize the dispersion property of the waveguide as needed. We believe this dispersion engineering approach can lead to promising applications in optical networks.

CHAPTER 6

CONCLUSION

This thesis provides a detailed explanation for taking advantage of the guided mode resonance in achieving the Goos-Hänchen shift from dielectric periodic structures rather than the homogeneous dielectric interfaces.

The advantage of the guided mode resonance by using dielectric gratings is to generate giant or mediocre Goos-Hänchen shift in both positive and negative directions. The guided mode resonance can also generate high quality factor resonance, which is a promising feature to realize low-threshold intensity bistability. We have shown that the grating can provide both phase and Goos-Hänchen shift bistability, which deserves further investigation of its features to evaluate the feasibility of many engineering applications. The capability to engineer the dispersion relation was also developed for the dielectric grating. Together with the negative GH shift, the grating can achieve a flat dispersion curve which corresponds to a "frozen mode". By changing the period of the grating, broadband light signal can be "frozen" inside the waveguide, forming a "trapped rainbow" for the visible spectrum.

The design examined in this thesis used dielectric periodic grating to achieve giant GH shift, especially negative ones that used to be obtained with high loss surface plasmonics and metamaterial. This dielectric design dramatically reduces the metallic loss and increases the portion among of GH shift that can be obtained. Therefore,we obtained a Goos-Hänchen shift corresponding to 5000 times of the wavelength, however, there does not seem to be a

theoretical upper bound. This GH shift based on guided mode resonance represents a good candidate for applications where high sensitivity is needed. Gigantic GH shift can be realized with high quality factor resonance and controlled by the grating parameters. Further, it can be implemented to obtain optical bistability in applications that require bistable phases or lateral shifts.

The abnormal reflection phase property of the grating can be taken advantage of to engineer the dispersion of a slab waveguide. It was proved that engineering the reflection phase of one or two sides of a common dielectric slab waveguide suffices to engineer the dispersion property. A flat dispersion curve was achieved as the "frozen" mode which corresponds to zero net energy flow. Also, it is mathematically verified using geometric optics by taking GH shift into account. Further, the numerical experiments explain the "frozen mode" in both frequency (RCWA) and time (FDTD) domain analysis. By tuning the horizontal parameter of the grating, the frequency of "frozen mode" can range over the entire visible spectrum. This ultra broad bandwidth indicates the great potential of the grating in dispersion engineering. The simplicity of the device configuration and low-loss material used improve the realization of the original trapped rainbow idea, which could contribute a building block to all-optical processing research.

APPENDICES

Appendix A

GENERAL SOLUTION FOR EM WAVES IN HOMOGENEOUS AND INHOMOGENEOUS MEDIA

All free space electromagnetism is governed by the four free space Maxwell equations, which are:

$$\begin{aligned} \nabla \cdot \mathbf{E} &= 0 & \nabla \times \mathbf{E} + \frac{\partial \mathbf{B}}{\partial t} &= 0 \\ \nabla \cdot \mathbf{B} &= \rho & \nabla \times \mathbf{H} - \frac{\partial \mathbf{D}}{\partial t} &= \mathbf{J} \end{aligned} \tag{A.1}$$

where $\mathbf{E}$ and $\mathbf{H}$ are the electric and magnetic fields, $\mathbf{D} = \epsilon\mathbf{E}$ and $\mathbf{B} = \mu\mathbf{H}$ are the electric displacement and magnetic induction fields. ρ and $\mathbf{J}$ are the free charge and current densities.

From Maxwell equations, the wave equation in homogeneous media can be derived ($\rho = 0$, $\mathbf{J} = 0$) as following

$$\nabla \times (\nabla \times \mathbf{E}) = \frac{\partial}{\partial t} \nabla \times \mathbf{B} = -\mu\epsilon \frac{\partial^2 \mathbf{E}}{\partial t^2} \tag{A.2}$$

with the relation of

$$\nabla \times (\nabla \times \mathbf{E}) = \nabla(\nabla \cdot E) - \nabla^2 \mathbf{E} = -\nabla^2 \mathbf{E} \tag{A.3}$$

Appendix A (Continued)

we can have electric field wave equation as:

$$\nabla^2\mathbf{E} - \frac{1}{c^2}\frac{\partial^2\mathbf{E}}{\partial t^2} = 0 \tag{A.4}$$

and similarly for magnetic field:

$$\nabla^2\mathbf{B} - \frac{1}{c^2}\frac{\partial^2\mathbf{B}}{\partial t^2} = 0 \tag{A.5}$$

Here, $c = 1/\sqrt{\mu\epsilon}$ is the speed of light in the media. In practice, many electromagnetic waves are approximated as time-harmonic sinusoids at a certain frequency. Even if the wave were not monochromatic, we can consider them as the superposition of multiple sinusoidal waves at different frequencies using Fourier analysis (35). Therefore time-harmonic monochromatic wave will be discussed in the following. The time harmonic fields are expressed as :

$$\mathbf{E}(\mathbf{r}, t) = \mathbf{E}(\mathbf{r})e^{-j\omega t} \tag{A.6a}$$

$$\mathbf{B}(\mathbf{r}, t) = \mathbf{B}(\mathbf{r})e^{-j\omega t} \tag{A.6b}$$

Follow the derivation above for time harmonic waves, we can achieve Helmholtz equation:

$$\nabla^2\mathbf{G} + k^2\mathbf{G} = 0 \tag{A.7}$$

$$k = \omega\sqrt{\mu\epsilon} \tag{A.8}$$

Appendix A (Continued)

here $\mathbf{G}$ stands for either electric or magnetic field. Note that Equation A.7 is equivalent to Equation A.3 only if $\nabla \cdot \mathbf{G} = 0$. A general solution for the electromagnetic wave is

$$\mathbf{G}(\mathbf{r}) = |G|e^{jkr} \tag{A.9}$$

The general solution applies to any media since it fulfills the requirements of Maxwell's equation. More sophisticated situation is inhomogeneous medium. The Maxwell equations for a source free inhomogeneous medium can be written as:

$$\begin{aligned} \nabla \cdot \mathbf{H}(\mathbf{r}, t) = 0 \qquad & \nabla \times \mathbf{E}(\mathbf{r}, t) + \mu_0 \frac{\partial \mathbf{H}(\mathbf{r}, \mathbf{t})}{\partial t} = 0 \\ \nabla \cdot [\epsilon(\mathbf{r})\mathbf{E}(\mathbf{r}, t)] = 0 \qquad & \nabla \times \mathbf{H}(\mathbf{r}, t) + \epsilon_0 \epsilon(\mathbf{r}) \frac{\partial \mathbf{E}(\mathbf{r}, \mathbf{t})}{\partial t} = 0 \end{aligned} \tag{A.10}$$

Here μ is generally considered as μ_0 for most dielectric material in optics frequencies, while $\epsilon(\mathbf{r})$ is a permitivitty function of the position. Due to the complexity of the material, a solution similar to Helmholtz equation cannot be achieved but result in a master equation as:

$$\nabla \left(\frac{1}{\epsilon(\mathbf{r})} \nabla \times \mathbf{H}(\mathbf{r}) \right) = \left(\frac{\omega}{c} \right)^2 \mathbf{H}(\mathbf{r}) \tag{A.11}$$

Together with the divergence equations in Equation A.10, the property of the electromagnetic wave can be revealed. The strategy is as follows: for a given structure of $\epsilon(\mathbf{r})$, we can solve the eigenmode $\mathbf{H}(\mathbf{r})$ for the master equation Equation A.11. $\mathbf{H}(\mathbf{r})$ is the eigenvector which depicts

Appendix A (Continued)

the spatial patterns of the time harmonic modes with eigenvalues $(\omega/c)^2$. Then use the fourth equation in Equation A.10 to recover $\mathbf{E}(\mathbf{r})$:

$$\mathbf{E}(\mathbf{r}) = \frac{j}{\omega\epsilon_0\epsilon(\mathbf{r})}\nabla \times \mathbf{H}(\mathbf{r}) \tag{A.12}$$

However, practical analysis via this approach could be computationally difficult. Particular analysis will be demonstrated when periodicity or other constraints are introduced.

Appendix B

DISCLAIMER FOR REPRODUCTION

Chapter 3 and Chapter 5 are reproduced from the author's publications shown below, respectively. The reproduction is permitted by Optical Society of America.

- Rui Yang, Wenkan Zhu and Jingjing Li, "Giant positive and negative Goos-Hänchen shift caused by guided mode resonance",Optics Express 22, 2043-2050 (2014)
- Rui Yang, Wenkan Zhu and Jingjing Li, "Realization of trapped rainbow in 1D slab waveguide with surface dispersion engineering" Optics Express 23, 6326-6335 (2015)

Permission from Optical Society of America

pubscopyright Feb 10

Dear Rui Yang,

Thank you for contacting The Optical Society.

Because you are the author of the source paper from which you wish to reproduce material, OSA considers your requested use of its copyrighted materials to be permissible within the author rights granted in the Copyright Transfer Agreement submitted by the requester on acceptance for publication of his/her manuscript. It is requested that a complete citation of the original material be included in any publication. This permission assumes that the material was not reproduced from another source when published in the original publication.

Please let me know if you have any questions.

Appendix B (Continued)

Kind Regards,

Susannah Lehman

Authorized Agent, The Optical Society

CITED LITERATURE

1. Goos, F. and Hänchen, H.: "Ein neuer und fundamentaler Versuch zur Totalreflexion". Annalen der Physik, 436(7-8):333–346, 1947.

2. Artmann, K.: . Annalen der Physik 6, 2:87, 1948.

3. Goos, F. and Lindberg-Hänchen, H.: "Neumessung des Strahlversetzungseffektes bei Totalreflexion". Annalen der Physik, 440:251–252, 1949.

4. Wolter, H., N. Z.: . Optik, 5a:143, 1950.

5. Burke, J.: . Optical Science Newsletter (Univ. Arizona), 5:31, 1971.

6. Tamir, T. and Bertoni, H. L.: "Lateral Displacement of Optical Beams at Multilayered and Periodic Structures". Journal of the Optical Society America, 61(10):1397–1413, October 1971.

7. Shadrivov, I. V., Zharov, A. A., and Kivshar, Y. S.: "Giant Goos-Hänchen effect at the reflection from left-handed metamaterials". Applied Physics Letters, 83(13):2713–2715, September 2003.

8. Bonnet, C., Chauvat, D., Emile, O., Bretenaker, F., Le Floch, A., and Dutriaux, L.: "Measurement of positive and negative Goos–Hänchen effects for metallic gratings near Wood anomalies". Optics Letters, 26(10):666–668, May 2001.

9. Mateus, C., Huang, M., Chen, L., Chang-Hasnain, C., and Suzuki, Y.: "Broad-band mirror (1.12-1.62 μ m) using a subwavelength grating". IEEE Photonics Technology Letters, 16(7):1676–1678, July 2004.

10. Mateus, C. F., Huang, M. C., Deng, Y., Neureuther, A. R., and Chang-Hasnain, C. J.: "Ultrabroadband mirror using low-index cladded subwavelength grating". IEEE Photonics Technology Letters, 16(2):518–520, February 2004.

11. Wang, S. S. and Magnusson, R.: "Theory and applications of guided-mode resonance filters". Applied Optics, 32(14):2606–2613, May 1993.

CITED LITERATURE (Continued)

12. Born, M. and Wolf, E.: "Principles of Optics: Electromagnetic Theory of Propagation, Interference and Diffraction of Light". Cambridge University Press, October 1999.

13. Horowitz, B. R. and Tamir, T.: "Lateral displacement of a light beam at a dielectric interface". Journal of the Optical Society America, 61:586, 1971.

14. Lai, H. M., Kwok, C. W., Loo, Y. W., and Xu, B. Y.: "Energy-flux pattern in the Goos-Hänchen effect". Physical Review E, 62(5):7330–7339, November 2000.

15. Renard, R. H.: "Total reflection: a new evaluation of the goos-hänchen shift". Journal of Optical Society America, 54(10):1190–1196, October 1964.

16. Lotsch, H. K. V.: "Reflection and refraction of a beam of light at a plane interface". Journal of the Optical Society of America, 58(4):551–561, April 1968.

17. Carniglia, C. K.: "Correction to the theory of the Goos-Hänchen shift by Lotsch". Journal of the Optical Society America, 66:12, 1976.

18. Anicin, B. A., Fazlic, R., and Kopric, M.: "Theoretical evidence for negative Goos-Hänchen shifts". Journal of Physics A: Mathematical and General, 11(8):1657, August 1978.

19. Wild, W. J. and Giles, C. L.: "Goos-Hänchen shifts from absorbing media". Physical Review A, 25(4):2099–2101, April 1982.

20. Lai, H. M. and Chan, S. W.: "Large and negative Goos-Hänchen shift near the Brewster dip on reflection from weakly absorbing media". Optics Letters, 27(9):680–682, May 2002.

21. Berman, P. R.: "Goos-Hänchen shift in negatively refractive media". Physical Review E, 66(6):067603, December 2002.

22. Yin, X., Hesselink, L., Liu, Z., Fang, N., and Zhang, X.: "Large positive and negative lateral optical beam displacements due to surface plasmon resonance". Applied Physics Letters, 85(3):372, 2004.

23. Wang, L.-G., Chen, H., and Zhu, S.-Y.: "Large negative Goos-Hänchen shift from a weakly absorbing dielectric slab". Optical Letters, 30(21):2936–2938, 2005.

24. He, J., Yi, J., and He, S.: "Giant negative Goos-Hänchen shifts for a photonic crystal with a negative effective index". Optics Express, 14(7):3024–3029, April 2006.

CITED LITERATURE (Continued)

25. Leung, P., Chen, C., and Chiang, H.-P.: "Large negative Goos-Hänchen shift at metal surfaces". Optics Communications, 276(2):206–208, August 2007.

26. Merano, M., Aiello, A., Hooft, G. W., van Exter, M. P., Eliel, E. R., and Woerdman, J. P.: "Observation of Goos-Hänchen shifts in metallic reflection". Optics Express, 15(24):15928–15934, November 2007.

27. Tamir, T. and Garmire, E.: "Integrated optics". Berlin; New York, Springer-Verlag, 1979.

28. Tamir, T.: "Nonspecular phenomena in beam fields reflected by multilayered media". Journal of the Optical Society America A, 3(4):558 – 565, 1986.

29. Breazeale, M. A. and Torbett, M. A.: "Backward displacement of waves reflected from an interface having superimposed periodicity". Applied Physics Letters, 29(8):456, October 1976.

30. Teklu, A., Breazeale, M. A., Declercq, N. F., Hasse, R. D., and McPherson, M. S.: "Backward displacement of ultrasonic waves reflected from a periodically corrugated interface". Journal of Applied Physics, 97, April 2005.

31. Herbison, S. W., Vander Weide, J. M., and Declercq, N. F.: "Observation of ultrasonic backward beam displacement in transmission through a solid having superimposed periodicity". Applied Physics Letters, 97(4):041908, July 2010.

32. Huang, M. C. Y., Zhou, Y., and Chang-Hasnain, C. J.: "A surface-emitting laser incorporating a high-index-contrast subwavelength grating". Nature Photonics, 1(2):119–122, February 2007.

33. Magnusson, R. and Wang, S. S.: "New principle for optical filters". Applied Physics Letters, 61(9):1022–1024, August 1992.

34. Fattal, D., Li, J., Peng, Z., Fiorentino, M., and Beausoleil, R. G.: "Flat dielectric grating reflectors with focusing abilities". Nature Photonics, 4(7):466–470, July 2010.

35. Stratton, J., Antennas, I., and Society, P.: "Electromagnetic Theory". An IEEE Press classic reissue. Wiley, 2007.

36. Borgnis, F. and Papas, C.: Electromagnetic waveguides and resonators. Springer, 1958.

CITED LITERATURE (Continued)

37. Li, L.: "New formulation of the Fourier modal method for crossed surface relief gratings". Journal of the Optical Society America A, 14(10):2758–2767, 1997.

38. Oskooi, A., Roundy, D., Ibanescu, M., Bermel, P., Joannopoulos, J., and Johnson, S.: "MEEP: A flexible free-software package for electromagnetic simulations by the FDTD method". Computer Physics Communications, 181(3):687–702, 2010.

39. Coggon, J. H.: "Electromagnetic and electrical modeling by the finite element method". Geophysics, 36(1):132–155, 1971.

40. Peng, S., Tamir, T., and Bertoni, H. L.: "Theory of periodic dielectric waveguides". IEEE Transactions on Microwave Theory and Techniques, 23(1):123–133, January 1975.

41. Morse, P. M. . and Feshbach, H.: "Methods Of Theoretical Physics". New York: McGraw-Hill, 1953.

42. Floquet, G.: "Sur les équations différentielles linéaires à coefficients pŕiodiques". Annales de l'École Normale Supérieure, 12:47–88, 1883.

43. Gazalet, J., Dupont, S., Kastelik, J., Rolland, Q., and Djafari-Rouhani, B.: "a tutorial survey on waves propagating in periodic media: Electronic, photonic and phononic crystals. perception of the bloch theorem in both real and fourier domains". Wave Motion, 50(3):619 – 654, 2013.

44. Li, L.: "Use of Fourier series in the analysis of discontinuous periodic structures". Journal of the Optical Society of America A, 13(9):1870.

45. Yin, X. and Hesselink, L.: "Goos-Hänchen shift surface plasmon resonance sensor". Applied Physics Letters, 89(26):261108, December 2006.

46. Chen, C.-W., Lin, W.-C., Liao, L.-S., Lin, Z.-H., Chiang, H.-P., Leung, P.-T., Sijercic, E., and Tse, W.-S.: "Optical temperature sensing based on the Goos-Hänchen effect". Applied Optics, 46(22):5347, August 2007.

47. Marburger, J. H. and Felber, F. S.: "Theory of a lossless nonlinear Fabry-Pérot interferometer". Physical Review A, 17(1):335–342, January 1978.

48. Gibbs, H.: "Optical bistability: controlling light with light". Elsevier, 2012.

CITED LITERATURE (Continued)

49. Gibbs, H. M., McCall, S. L., and Venkatesan, T. N. C.: "Differential gain and bistability using a Sodium-filled Fabry-Pérot interferometer". Physical Review Letters, 36(19):1135–1138, May 1976.

50. Smith, P. W. and Turner, E. H.: "A bistable Fabry-Pérot resonator". Applied Physics Letters, 30(6):280–281, August 2008.

51. Ngo, Q. M., Le, K. Q., and Lam, V. D.: "Optical bistability based on guided-mode resonances in photonic crystal slabs". Journal of the Optical Society of America B, 29(6):1291–1295, June 2012.

52. Radic, S., George, N., and Agrawal, G. P.: "Optical switching in $\lambda/4$-shifted nonlinear periodic structures". Optics Letters, 19(21):1789–1791, November 1994.

53. Yanik, M. F., Fan, S., Soljacic, M., and Joannopoulos, J. D.: "All-optical transistor action with bistable switching in a photonic crystal cross-waveguide geometry". Optics Letters, 28(24):2506–2508, December 2003.

54. Daniel, B. and Agrawal, G.: "Phase-switched all-optical flip-flops using two-input bistable resonators". IEEE Photonics Technology Letters, 24(6):479–481, March 2012.

55. Soler, A. D. and Udoev, Y. P.: "Optical bistability and modulation of light in a thin-film resonator based on total internal reflection". Technical Physics, 42(12):1406–1410, December 1997.

56. Vincent, P., Paraire, N., Neviere, M., Koster, A., and Reinisch, R.: "Gratings in nonlinear optics and optical bistability". Journal of the Optical Society of America B, 2(7):1106–1116, July 1985.

57. Ngo, Q. M., Kim, S., Song, S. H., and Magnusson, R.: "Optical bistable devices based on guided-mode resonance in slab waveguide gratings". Optics Express, 17(26):23459–23467, December 2009.

58. Soljacic, M., Ibanescu, M., Luo, C., Johnson, S. G., Fan, S., Fink, Y., and Joannopoulos, J. D.: "All-optical switching using optical bistability in nonlinear photonic crystals". Proc. SPIE 5000, Photonic Crystal Materials and Devicess, pages 200–214, July 2003.

CITED LITERATURE (Continued)

59. Wei, R.-R., Chen, X., Tao, J.-W., and Li, C.-F.: "Giant and negative bistable shifts for one-dimensional photonic crystal containing a nonlinear metamaterial defect". Physics Letters A, 372(45):6797–6800, November 2008.

60. Chen, X., Wei, R.-R., Shen, M., Zhang, Z.-F., and Li, C.-F.: "Bistable and negative lateral shifts of the reflected light beam from Kretschmann configuration with nonlinear left-handed metamaterials". Applied Physics B, 101(1-2):283–289, October 2010.

61. Wang, X., Jiang, A., and Zheng, F.: "Large and bistable Goos-Hänchen shifts from the Kretschmann configuration with a nonlinear negative-zero-positive index metamaterial". Journal of Optics, 16(4):045101, April 2014.

62. Yang, R., Zhu, W., and Li, J.: "Giant positive and negative Goos-Hänchen shift on dielectric gratings caused by guided mode resonance". Optics Express, 22(2):2043–2050, January 2014.

63. Yang, R., Zhu, W., and Li, J.: Realization of trapped rainbow in 1d slab waveguide with surface dispersion engineering. Optics Express, 23(5):6326–6335, March 2015.

64. Reinisch, R. and Vitrant, G.: "Optical bistability". Progress in Quantum Electronics, 18(1):1–38, January 1994.

65. Zhou, Y., Moewe, M., Kern, J., Huang, M. C. Y., and Chang-Hasnain, C. J.: "Surface-normal emission of a high-Q resonator using a subwavelength high-contrast grating". Optics Express, 16(22):17282–17287, October 2008.

66. D'Aguanno, G., d. C. D. M. N. and Bloemer, M. J.: "All-optical switching at the Fano resonances in subwavelength gratings with very narrow slits". Optical Letters, 36(11):1984–1986, June 2011.

67. Hau, L. V., Harris, S. E., Dutton, Z., and Behroozi, C. H.: "Light speed reduction to 17 metres per second in an ultracold atomic gas". Nature, 397(6720):594–598, February 1999.

68. Ma, P. S., Kwon, Y. E., and Kim, Y. Y.: "Wave dispersion tailoring in an elastic waveguide by phononic crystals". Applied Physics Letters, 103(15):151901, October 2013.

69. Li, J., White, T. P., O'Faolain, L., Gomez-Iglesias, A., and Krauss, T. F.: "Systematic design of flat band slow light in photonic crystal waveguides". Optics Express, 16(9):6227–6232, April 2008.

CITED LITERATURE (Continued)

70. Schulz, S. A., O'Faolain, L., Beggs, D. M., White, T. P., Melloni, A., and Krauss, T. F.: "Dispersion engineered slow light in photonic crystals: a comparison". Journal of Optics, 12(10):104004, October 2010.

71. Colman, P., Combriè, S., Lehoucq, G., and De Rossi, A.: "Control of dispersion in photonic crystal waveguides using group symmetry theory". Optics Express, 20(12):13108–13114, June 2012.

72. Tsakmakidis, K. L., Boardman, A. D., and Hess, O.: " "Trapped rainbow" storage of light in metamaterials". Nature, 450(7168):397–401, November 2007.

73. Gan, Q., Gao, Y., Wagner, K., Vezenov, D., Ding, Y. J., and Bartoli, F. J.: "Experimental verification of the rainbow trapping effect in adiabatic plasmonic gratings". Proceedings of the National Academy of Sciences, 108(13):5169–5173, March 2011.

74. Gan, Q. and Bartoli, F. J.: "Surface dispersion engineering of planar plasmonic chirped grating for complete visible rainbow trapping". Applied Physics Letters, 98(25):251103, June 2011.

75. Smolyaninova, V. N., Smolyaninov, I. I., Kildishev, A. V., and Shalaev, V. M.: "Experimental observation of the trapped rainbow". Applied Physics Letters, 96(21):211121, 2010.

76. see http://www.fourmilab.ch/documents/specrend/.

77. Mandelshtam, V. A. and Taylor, H. S.: "Harmonic inversion of time signals and its applications". Journal of Chemical Physics, 107(17):6756, 1997.

VITA

NAME:	Rui Yang
EDUCATION:	Ph.D. in Electrical and Computer Engineering, University of Illinois at Chicago, 2016 M.S. in Physics, University of Illinois at Chicago, 2012 B.S. in Physics, Shandong University, China, 2011
EXPERIENCE:	Research Assistant, August 2011 to May 2016 Teaching Assistant and Lecturer, August 2011 to May 2016
JOURNAL PAPERS:	R. Yang, W. Zhu and J. Li, "Giant positive and negative Goos-Hänchen shift caused by guided mode resonance",Optics Express 22, 2043-2050 (2014) R. Yang, W. Zhu and J. Li, "Realization of trapped rainbow in 1D slab waveguide with surface dispersion engineering" Optics Express 23, 6326-6335 (2015)
CONFERENCE PAPERS:	R. Yang and J. Li, Trapping a rainbow with 1D dielectric slab waveguide, Antennas and Propagation Society International Symposium (APSURSI), pp. 348-349, 2014